13 Propagation, Modulation, and Oscillation in Optical Dielectric Waveguides

13.0 INTRODUCTION

In this chapter we discuss a number of topics that involve propagation of optical modes in dielectric films with thicknesses comparable to the wavelength.

The ability to generate, guide, modulate, and detect light in such thin film configurations [1–3] opens up new possibilities for monolithic "optical circuits" [4]—an endeavor going under the name of integrated optics [5].

We will first consider the basic problem of TE and TM mode propagation in slab dielectric waveguides. A coupled-mode formalism is then developed to describe situations involving exchange of power between modes. These include (a) periodic (corrugated) optical waveguides and filters, (b) distributed feedback lasers, (c) electrooptic mode coupling, and (d) directional couplers.

13.1 WAVEGUIDE MODES—A GENERAL DISCUSSION

A prerequisite to understanding guided wave interactions is a knowledge of the properties of the guided modes. A mode of a dielectric waveguide at a (radian) frequency ω is a solution of the wave equation

$$\nabla^2\mathbf{E}(\mathbf{r}) + k_0^2 n^2(\mathbf{r})\mathbf{E}(\mathbf{r}) = 0 \qquad (13.1\text{-}1)$$

where $k_0^2 \equiv \omega^2\mu\varepsilon_0 = (2\pi/\lambda)^2$ and n is the index of refraction. The solutions are subject to the continuity of the tangential components of $\mathbf{E}$ and $\mathbf{H}$ at the

dielectric interfaces. In (13.1-1) the form of the field is taken as

$$\mathbf{E}(\mathbf{r}, t) = \mathbf{E}(x, y)e^{i(\omega t - \beta z)} \tag{13.1-2}$$

so that (13.1-1) becomes

$$\left(\frac{\partial^2}{\partial x^2} + \frac{\partial^2}{\partial y^2}\right)\mathbf{E}(x, y) + [k_0^2 n^2(\mathbf{r}) - \beta^2]\mathbf{E}(x, y) = 0 \tag{13.1-3}$$

The basic features of the behavior of dielectric waveguides can be elucidated with the help of a slab (planar) model in which no variation exists in one (for example, y) dimension. Channel waveguides, in which the waveguide dimensions are finite in both the x and y directions, approach the behavior of the planar guide when one dimension is considerably larger than the other [6, 7]. Even when this is not the case, most of the phenomena of interest are only modified in a simple quantitative way when going from a planar to a channel waveguide. Because of the immense mathematical simplification that results, we will limit most of the following treatment to planar waveguides such as the one shown in Figure 13-1.

Putting $\partial/\partial y = 0$ in (13.1-3) and writing it separately for regions I, II, and III yields

Region I
$$\frac{\partial^2}{\partial x^2} E(x, y) + (k_0^2 n_1^2 - \beta^2)E(x, y) = 0 \tag{13.1-4a}$$

Region II
$$\frac{\partial^2}{\partial x^2} E(x, y) + (k_0^2 n_2^2 - \beta^2)E(x, y) = 0 \tag{13.1-4b}$$

Region III
$$\frac{\partial^2}{\partial x^2} E(x, y) + (k_0^2 n_3^2 - \beta^2)E(x, y) = 0 \tag{13.1-4c}$$

where $E(x, y)$ is a Cartesian component of $\mathbf{E}(x, y)$. Before embarking on a formal solution of (13.1-4), we may learn a great deal about the physical nature of the solutions by simple arguments. Let us consider the nature of the solutions as a function of the propagation constant β at a *fixed* frequency ω. Let us assume that $n_2 > n_3 > n_1$. For $\beta > k_0 n_2$ [that is, regime (a) in Figure 13-2], it follows directly from (13.1-4) that $(1/E)(\partial^2 E/\partial x^2) > 0$ everywhere, and $E(x)$ is exponential in all three layers (I, II, III) of the waveguides. Because of the need to match both $E(x)$ and its derivatives at the two interfaces, the resulting field distribution is as shown in Figure 13-2(a). The

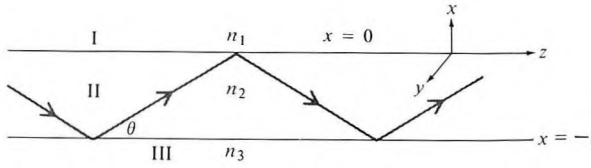

Figure 13-1 A slab ($\partial/\partial y = 0$) dielectric waveguide.

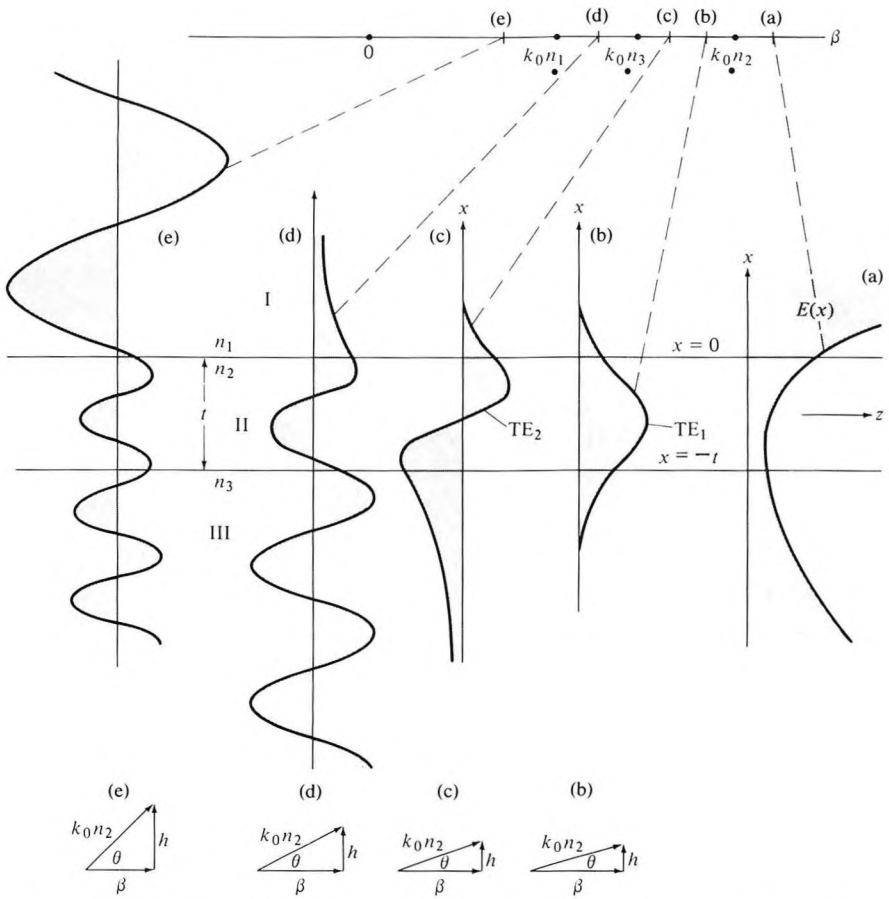

Figure 13-2 (*top*) The different regimes (a, b, c, d, e) of the propagation constant, β, of the waveguide shown in Figure 13-1. (*middle*) The field distributions corresponding to the different value of β. (*bottom*) The propagation triangles corresponding to the different propagation regimes.

field increases without bound away from the waveguide so that the solution is not *physically realizable* and thus does not correspond to a real wave.

For $k_0n_3 < \beta < k_0n_2$, as in points (b) and (c), it follows from (13.1-4) that the solution is sinusoidal in region II, since $(1/E)(\partial^2E/\partial x^2) < 0$, but is exponential in regions I and III. This makes it possible to have a solution $E(x)$ that satisfies the boundary conditions while *decaying* exponentially in regions I and III. Two such solutions are shown in Figure 13-2(b) and (c). The energy carried by these modes is confined to the vicinity of the guiding layer II, and we will, consequently, refer to them as confined, or guided, modes. From the above discussion it follows that a necessary condition for their existence is that k_0n_1, $k_0n_3 < \beta < k_0n_2$ so that confined modes are

possible only when $n_2 > n_1, n_3$; that is, the inner layer possesses the highest index of refraction.

Mode solutions for $k_0 n_1 < \beta < k_0 n_3$, regime (d), correspond according to (13.1-4) to exponential behavior in region I and to sinusoidal behavior in regions II and III as illustrated in Figure 13-2(d). We will refer to these modes as substrate radiation modes. For $0 < \beta < k_0 n_1$, as in (e), the solution for $E(x)$ becomes sinusoidal in all three regions. These are the so-called radiation modes of the waveguides.

A solution of (13.1-4) subject to the boundary conditions at the interfaces given in the next section shows that while in regimes (d) and (e) β is a continuous variable, the values of allowed β in the propagation regime $k_0 n_3 < \beta < k_0 n_2$ are *discrete*. The number of confined modes depends on the width, t, the frequency, and the indices of refraction n_1, n_2, n_3. At a given wavelength the number of confined modes increases from 0 with increasing t. At some t, the mode TE_1 becomes confined. Further increases in t will allow TE_2 to exist as well, and so on.

A useful point of view is one of considering the wave propagation in the inner layer 2 as that of a plane wave propagating at some angle θ to the horizontal axis and undergoing a series of total internal reflections at the interfaces II–I and II–III. This is based on (13.1-4b). Assuming a solution in the form of $E \propto \sin(hx + \alpha) \exp(-i\beta z)$, we obtain

$$\beta^2 + h^2 = k_0^2 n_2^2 \qquad (13.1\text{-}5)$$

The resulting right-angle triangles with sides β, h, and $k_0 n_2$ are shown in Figure 13-2. Note that since the frequency is constant, $k_0 n_2 \equiv (\omega/c) n_2$ is the same for cases (b), (c), (d), and (e). The propagation can thus be considered formally as that of a plane wave along the direction of the hypotenuse with a *constant* propagation constant $k_0 n_2$. As β decreases, θ increases until, at $\beta = k_0 n_3$, the wave ceases to be totally internally reflected at the interface III–II. This follows from the fact that the guiding condition $\beta > k_0 n_3$ leads, using $\beta = k_0 n_2 \cos\theta$, to $\theta < \cos^{-1}(n_3/n_2) = \theta_c$, where θ_c is the total internal reflection angle at the interface between layers II–III. Since $n_3 > n_1$, total internal reflection at the II–III interface guarantees total internal reflection at the I–II interface.

Confined Modes in a Symmetric Slab Waveguide

Before considering the more general, and difficult, case of asymmetric waveguides, we will solve in some detail the case of the symmetric slab waveguide where $n_1 = n_3$. The guiding layer of index $n_2 > n_1$ occupies the region $-d < x < d$, as in Figure 13-3.

We consider the case of harmonic time behavior in the form of $\exp(i\omega t)$ and in infinite slab geometry so that there is no variation in the y directions ($\partial/\partial y = 0$). Maxwell's equations (1.2-1) and (1.2-2) become

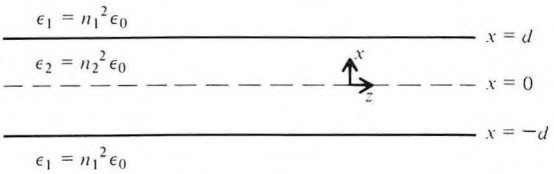

Figure 13-3 A symmetric slab waveguide.

$$\frac{\partial E_y}{\partial z} = i\omega\mu H_x \tag{13.1-6a}$$

$$\frac{\partial E_x}{\partial z} - \frac{\partial E_z}{\partial x} = -i\omega\mu H_y \tag{13.1-6b}$$

$$\frac{\partial E_y}{\partial x} = -i\omega\mu H_z \tag{13.1-6c}$$

$$\frac{\partial H_y}{\partial z} = -i\omega\varepsilon E_x \tag{13.1-6d}$$

$$\frac{\partial H_x}{\partial z} - \frac{\partial H_z}{\partial x} = i\omega\varepsilon E_y \tag{13.1-6e}$$

$$\frac{\partial H_y}{\partial x} = i\omega\varepsilon E_z \tag{13.1-6f}$$

Next we assume that the modes propagate in the z direction with the z dependence in the form of $\exp(-i\beta z)$ so that in (13.1-6) we can replace $\partial/\partial z$ by $-i\beta$. An inspection of (13.1-6) reveals that we may obtain two self-consistent types of solutions. The first contains only E_y, H_x, and H_z and is referred to as transverse electric (TE) modes, since the electric field (E_y) is restricted to the transverse (that is, normal to the direction of propagation) plane. Maxwell's equations (13.1-6) for the TE modes reduce to

$$E_y = -\frac{\omega\mu}{\beta} H_x \tag{13.1-7a}$$

$$\frac{\partial E_y}{\partial x} = -i\omega\mu H_z \tag{13.1-7b}$$

The second type of mode is transverse magnetic (TM) and involves H_y, E_x, and E_z. These are related, according to (13.1-6), by

$$H_y = \frac{\omega\varepsilon}{\beta} E_x \tag{13.1-8a}$$

$$E_z = -\frac{i}{\omega\varepsilon}\frac{\partial H_y}{\partial x} \tag{13.1-8b}$$

The solutions for the TE and TM modes are basically similar, so that in order to be specific we will consider the case of TE modes. Since the waveguide is symmetric about the plane $x = 0$, the mode solutions must be either even or odd in x, that is,

$$E_y(x, z, t) = E_y(-x, z, t)$$

in the case of even modes and

$$E_y(x, z, t) = -E_y(-x, z, t)$$

for the odd modes. The solution for the even modes is taken in the form

$$E_y = A \exp [-p(|x| - d) - i\beta z] \qquad |x| \geq d \tag{13.1-9}$$

and

$$E_y = B \cos (hx) \exp (-i\beta z) \qquad |x| \leq d \tag{13.1-10}$$

where p and h are positive real constants to be determined. From (13.1-7b) we obtain

$$H_z = \mp \frac{ipA}{\omega\mu} \exp [-p(|x| - d) - i\beta z] \qquad |x| \geq d \tag{13.1-11}$$

the $(-)$ sign is used with $x \geq d$ and $(+)$ for $x \leq -d$

$$H_z = -\frac{ihB}{\omega\mu} \sin (hx) \exp (-i\beta z) \qquad |x| \leq d \tag{13.1-12}$$

Next we require that the tangential field components E_y and H_z be continuous across the interfaces.[1] The continuity of E_y at $x = \pm d$ leads according to (13.1-9) and (13.1-10) to

$$A = B \cos (hd) \tag{13.1-13}$$

while the continuity of H_z results in

$$pA = hB \sin (hd) \tag{13.1-14}$$

From (13.1-13) and (13.1-14) it follows that

$$pd = hd \tan (hd) \tag{13.1-15}$$

Since the field solutions (13.1-9) and (13.1-10) must satisfy the wave equation (13.1-4a,b), the following relations are obeyed

$$\beta^2 = k_0^2 n_2^2 - h^2$$

$$\beta^2 = k_0^2 n_1^2 + p^2 \tag{13.1-16}$$

[1]The reasons for these conditions are discussed in any elementary text on electromagnetic theory.

The last two equations can be combined to give

$$(pd)^2 + (hd)^2 = (n_2^2 - n_1^2)k_0^2 d^2 \tag{13.1-17}$$

The propagation constants p and h of a given mode need to satisfy, simultaneously, (13.1-15) and (13.1-17). A straightforward graphical solution is illustrated by Figure 13-4 and consists of finding the intersections in the pd-hd plane of the circle $(pd)^2 + (hd)^2 = (n_2^2 - n_1^2)k_0^2 d^2$ with the curve $pd = hd \tan(hd)$. Each intersection with a $p > 0$ corresponds to a confined mode. The propagation constant β of a given mode can be obtained, once p and h are given, from (13.1-16).

To appreciate the nature of the solutions, let us consider what happens in a given waveguide (that is, fixed n_1, n_2, and d) as the frequency increases gradually from zero. Since $k_0 = \omega/c$, the effect of increasing the frequency is to increase the radius of the circle $(pd)^2 + (hd)^2 = (n_2^2 - n_1^2)k_0^2 d^2$. At low frequencies such that

$$0 < \sqrt{n_2^2 - n_1^2}\, k_0 d < \pi \tag{13.1-18}$$

only one intersection (point A) exists between the circle and the curve $pd = hd \tan(hd)$ with $p > 0$. This is evident from an inspection of Figure 13-4. The mode is designated as TE_1 and has a tranverse h parameter falling within the range

$$0 < h_1 d < \frac{\pi}{2} \tag{13.1-19}$$

so that it has no zero crossings in the interior of the slab $|x| \leq d$.

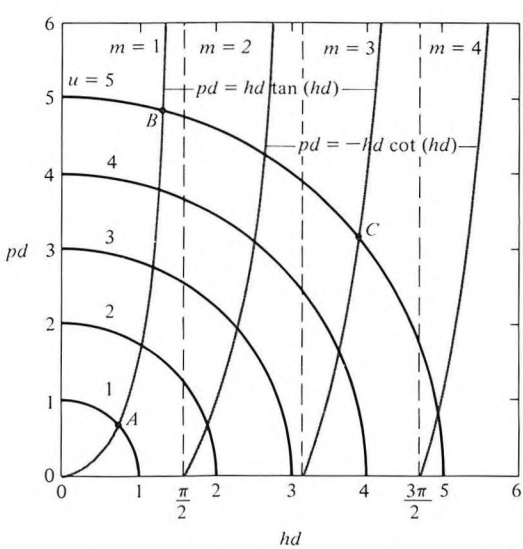

Figure 13-4 Plot of eigenvalue equations $pd = hd \tan(hd)$ for even TE modes, $pd = -hd \cot(hd)$ for odd TE modes, and the supplementary relationship $(pd)^2 + (hd)^2 = (n_2^2 - n_1^2)(k_0 d)^2 \equiv u^2$. (After Reference [8].)

When the parameter $u \equiv \sqrt{n_2^2 - n_1^2}k_0 d$ falls within the range

$$\pi < \sqrt{n_2^2 - n_1^2}k_0 d < 2\pi \tag{13.1-20}$$

we obtain two intersections with $p > 0$. One (point B) corresponds to a value of $hd < \pi/2$ and is thus that of the lowest order TE_1 mode. In the second mode (point C)

$$\pi < h_3 d < \frac{3\pi}{2} \tag{13.1-21}$$

and consequently this mode has two zero crossings (that is, points where $E_y = 0$) in the region $|x| < d$. This is the so-called TE_3 mode ($m = 3$ in Figure 13-4). Both of these modes correspond to the same frequency and can thus be excited simultaneously by the same input field. We notice, however, that the TE_1 mode has a larger value of p (that is, $p_1 > p_3$) and is therefore more highly confined to the interior slab. It also follows from (13.1-16) that $\beta_1 > \beta_3$, so that the phase velocity $v_1 = \omega/\beta_1$ of the TE_1 mode is smaller than that of the TE_3 mode.

From (13.1-19) and (13.1-21) one would conclude that no mode exists with $\pi/2 < hd < \pi$. This is due to the fact that up to this point, we considered only modes with even x symmetry as in (13.1-10). Another family of modes—the odd TE modes—exists and is described by

$$E_y = \begin{cases} A \exp\left[-p(x - d) - i\beta z\right] & x \geq d \\ -A \exp\left[p(x + d) - i\beta z\right] & x \leq -d \end{cases} \tag{13.1-22}$$

$$E_y = B \sin(hx) \exp(-i\beta z) \qquad |x| \leq d \tag{13.1-23}$$

Applying the continuity conditions at $|x| = d$ leads to

$$pd = -hd \cot(hd) \tag{13.1-24}$$

instead of (13.1-15). The mode solutions correspond to the intersection of (13.1-24) with the circle (13.1-17). Reference to Figure 13-4 shows that the corresponding values of h do indeed fill the gaps "avoided" by the even TE modes.

The lowest order odd TE mode is designated TE_2 ($m = 2$), since its h parameter h_2 satisfies

$$\frac{\pi}{2} < h_2 d < \pi \tag{13.1-25}$$

thus falling between h_1 (of TE_1) and h_3. We can now generalize and state that the mth (TE or TM) mode satisfies

$$(m - 1)\frac{\pi}{2} < h_m d < m\frac{\pi}{2} \tag{13.1-26}$$

and has $m - 1$ zero crossings in the internal region $|x| \leq d$. The modes 1,

3, 5, . . . are even symmetric, while those with $m = 2, 4, 6 \ldots$ are odd. We note that all the modes except the fundamental ($m = 1$) can exist (that is, are confined) only above a "cutoff" frequency. The higher the mode index, the higher its cutoff frequency. The fundamental mode can exist at any frequency, as is evident from Figure 13-4. If the dielectric waveguide is asymmetric ($n_1 \neq n_3$), the lowest order ($m = 1$) modes also possess a cutoff frequency. This case will be taken up in the next section.

The general features of TM modes are similar to those of TE modes except that the corresponding values of p are somewhat smaller, indicating a lesser degree of confinement. A larger fraction of the total TM mode power thus propagates in the outer media compared to a TE mode of the same order. This point is taken up in Problem 13.7.

13.2 TE AND TM MODES IN AN ASYMMETRIC SLAB WAVEGUIDE

In this section we will derive the mode solutions for the general asymmetric ($n_1 \neq n_3$) slab waveguide shown in Figure 13-1. We limit the derivation to the guided modes that according to Figure 13-2 have propagation constants β

$$k_0 n_3 < \beta < k_0 n_2$$

where, to be specific, $n_3 > n_1$.

TE modes

The field component E_y of the TE mode obeys the wave equation

$$\nabla^2 E_{yi}(x, y, z) + \omega^2 \mu \varepsilon_0 n_i^2 E_{yi} = 0 \qquad i = 1, 2, 3 \tag{13.2-1}$$

where i refers to the layer and the (real) electric field is given by

$$E_{yi}(x, y, z, t) = \text{Re}[E_{yi}(x, y, z) e^{i\omega t}]$$

For waves propagating along the z direction and for $\partial/\partial y = 0$ we have

$$E_{yi}(x, y, z) = \mathscr{E}_{yi}(x) e^{-i\beta z} \tag{13.2-2}$$

The transverse function $\mathscr{E}_{yi}(x)$ is taken as

$$\mathscr{E}_y = \begin{cases} C \exp(-qx) & 0 \leq x < \infty \\ C\left(\cos hx - \dfrac{q}{h} \sin hx\right) & -t \leq x \leq 0 \\ C\left(\cos ht + \dfrac{q}{h} \sin ht\right) \exp[p(x + t)] & -\infty < x \leq -t \end{cases} \tag{13.2-3}$$

Applying (13.2-1) to (13.2-3) results in

$$h = (n_2^2 k_0^2 - \beta^2)^{1/2}$$
$$q = (\beta^2 - n_1^2 k_0^2)^{1/2}$$
$$p = (\beta^2 - n_3^2 k_0^2)^{1/2}$$
$$k_0 \equiv \frac{\omega}{c} \tag{13.2-4}$$

The acceptable solutions for $\mathscr{E}_y$ and $\mathscr{H}_z = (i/\omega\mu)(\partial\mathscr{E}_y/\partial x)$ should be continuous at both $x = 0$ and $x = -t$. The choice of coefficients in (13.2-3) is such as to make $\mathscr{E}_y$ continuous at both interfaces as well as $(\partial\mathscr{E}_y/\partial x)$ at $x = 0$. By imposing the continuity requirement on $\partial\mathscr{E}_y/\partial x$ at $x = -t$, we get from (13.2-3)

$$h \sin ht - q \cos ht = p\left(\cos ht + \frac{q}{h} \sin ht\right)$$

or

$$\tan ht = \frac{p + q}{h(1 - pq/h^2)} \tag{13.2-5}$$

In the symmetric case ($n_1 = n_3$) the field (13.2-3) must be odd or even about the midplane $x = -t/2$. This special case was treated in Section 13.1 and leads to the eigenvalue equations (13.1-15) and (13.1-24). The last equation in conjunction with (13.2-4) is used to obtain the eigenvalues β for the confined TE modes. An example of such a solution is shown in Figure 13-5.

The constant, C, appearing in (13.2-3) is arbitrary, yet for many applications, especially those in which propagation and exchange of power involve more than one mode, it is advantageous to define C in such a way that it is simply related to total power in the mode. This point will become clear in Section 13.3. We choose C so that the field $\mathscr{E}_y(x)$ in (13.2-3) corresponds to a power flow of one watt (per unit width in y direction) in the mode. A mode for which $E_y = A\mathscr{E}_y(x)$ will thus correspond to a power flow of $|A|^2$ watts/m. The normalization condition becomes

$$-\frac{1}{2}\int_{-\infty}^{\infty} E_y H_x^* \, dx = \frac{\beta_m}{2\omega\mu}\int_{-\infty}^{\infty} [\mathscr{E}_y^{(m)}(x)]^2 \, dx = 1 \tag{13.2-6}$$

where the symbol m denotes the mth confined TE mode [corresponding to the mth eigenvalue of (13.2-5)] and $H_x = -i(\omega\mu)^{-1}\,\partial E_y/\partial z$.

Using (13.2-3) in (13.2-6) leads, after substantial but straightforward calculation, to

$$C_m = 2h_m\left(\frac{\omega\mu}{|\beta_m|[t + (1/q_m) + (1/p_m)](h_m^2 + q_m^2)}\right)^{1/2} \tag{13.2-7}$$

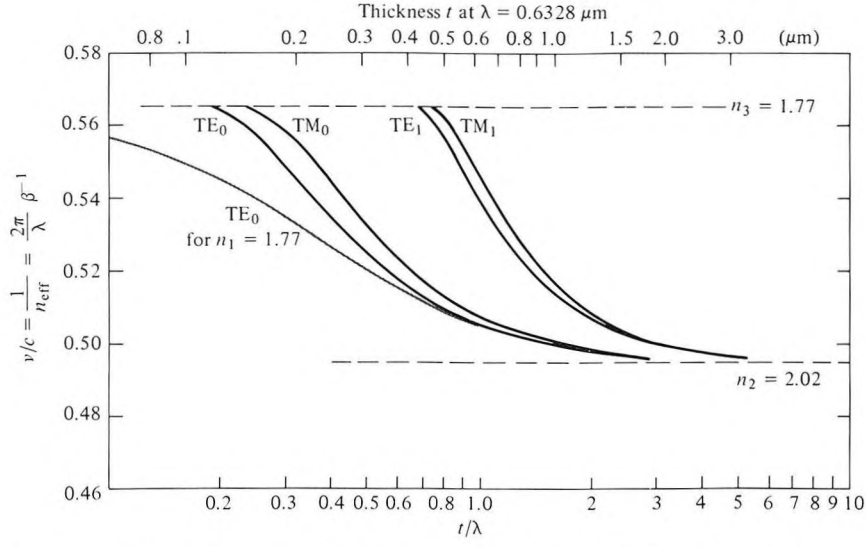

Figure 13-5 Dispersion curves for the confined modes of ZnO on sapphire waveguide $n_1 = 1$. (After Reference [10].)

Since the modes $\mathscr{E}_y^{(m)}$ are orthogonal (see Problem 13.6), we have

$$\int_{-\infty}^{\infty} \mathscr{E}_y^{(l)} \mathscr{E}_y^{(m)}\, dx = \frac{2\omega\mu}{\beta_m}\,\delta_{l,m} \tag{13.2-8}$$

TM modes

The derivation of the confined TM modes is similar in principle to that of the TE modes. Using (13.1-6) the field components are

$$\begin{aligned} H_y(x, z, t) &= \mathscr{H}_y(x) e^{i(\omega t - i\beta z)} \\ E_x(x, z, t) &= \frac{i}{\omega\varepsilon}\frac{\partial H_y}{\partial z} = \frac{\beta}{\omega\varepsilon}\,\mathscr{H}_y(x) e^{i(\omega t - \beta z)} \\ E_z(x, z, t) &= -\frac{i}{\omega\varepsilon}\frac{\partial H_y}{\partial x} \end{aligned} \tag{13.2-9}$$

The transverse function, $\mathscr{H}_y(x)$, is taken as

$$\mathscr{H}_y(x) = \begin{cases} -C\left(\dfrac{h}{\bar{q}}\cos ht + \sin ht\right) e^{p(x+t)} & x \le -t \\ C\left(-\dfrac{h}{\bar{q}}\cos hx + \sin hx\right) & -t \le x \le 0 \\ -\dfrac{h}{\bar{q}}\, Ce^{-qx} & x \ge 0 \end{cases} \tag{13.2-10}$$

The continuity of H_y and E_z at the two interfaces leads, in a manner similar to (13.2-5), to the eigenvalue equation

$$\tan ht = \frac{h(\bar{p} + \bar{q})}{h^2 - \bar{p}\bar{q}} \tag{13.2-11}$$

where

$$\bar{p} \equiv \frac{n_2^2}{n_3^2} p \qquad \bar{q} = \frac{n_2^2}{n_1^2} q$$

The normalization constant, C, is chosen so that the field represented by (13.2-9) and (13.2-10) carries *one* watt per unit width in the y direction

$$\frac{1}{2}\int_{-\infty}^{\infty} H_y E_x^* \, dx = \frac{\beta}{2\omega}\int_{-\infty}^{\infty} \frac{\mathcal{H}_y^2(x)}{\varepsilon(x)} \, dx = 1$$

or, using $n_i^2 \equiv \varepsilon_i/\varepsilon_0$,

$$\int_{-\infty}^{\infty} \frac{[\mathcal{H}_y^{(m)}(x)]^2}{n^2(x)} \, dx = \frac{2\omega\varepsilon_0}{\beta_m} \tag{13.2-12}$$

Carrying out the integration using (13.2-10) gives

$$C_m = 2\sqrt{\frac{\omega\varepsilon_0}{\beta_m t_{\text{eff}}}}$$

$$t_{\text{eff}} \equiv \frac{\bar{q}^2 + h^2}{\bar{q}^2}\left(\frac{t}{n_2^2} + \frac{q^2 + h^2}{\bar{q}^2 + h^2}\frac{1}{n_1^2 q} + \frac{p^2 + h^2}{\bar{p}^2 + h^2}\frac{1}{n_3^2 p}\right) \tag{13.2-13}$$

The general properties of the TE and TM mode solutions are illustrated in Figure 13-5. In general a mode becomes confined above a certain (cutoff) value of t/λ. At the cutoff value $p = 0$, and the mode extends to $x = -\infty$. For increasing values of t/λ, $p > 0$, and the mode becomes increasingly confined to layer 2. This is reflected in the effective mode index $\beta\lambda/2\pi$ that, at cutoff, is equal to n_3, and which, for large t/λ, approaches n_2. In a symmetric waveguide ($n_1 = n_3$) the lowest order modes TE_0 and TM_0 have no cutoff and are confined for all values of t/λ. The selective excitation of waveguide modes by means of prism couplers and a determination of their propagation constants β_m are described in Reference [11].

13.3 A PERTURBATION THEORY OF COUPLED MODES IN DIELECTRIC OPTICAL WAVEGUIDES

In Section 13.2 we obtained solutions for the confined modes supported by a slab dielectric waveguide such as that shown in Figure 13-1. An increasingly large number of experiments and devices involve coupling between such modes [12, 13, 17]. Typical examples are TM-to-TE mode conversion by

the electrooptic or acoustooptic effect [12] or coupling of forward-to-backward modes by means of a corrugation in one of the waveguides interfaces [15, 16]. In this section we will develop a formalism for describing such coupling.

We start with the Maxwell wave equation in the form

$$\nabla^2\mathbf{E}(\mathbf{r}, t) = \mu\epsilon_0 \frac{\partial^2\mathbf{E}(\mathbf{r}, t)}{\partial t^2} + \mu \frac{\partial^2}{\partial t^2} \mathbf{P}(\mathbf{r}, t) \tag{13.3-1}$$

The total medium polarization can be taken as the sum

$$\mathbf{P}(\mathbf{r}, t) = \mathbf{P}_0(\mathbf{r}, t) + \mathbf{P}_{\text{pert}}(\mathbf{r}, t) \tag{13.3-2}$$

where

$$\mathbf{P}_0(\mathbf{r}, t) = [\varepsilon(\mathbf{r}) - \varepsilon_0]\mathbf{E}(\mathbf{r}, t) \tag{13.3-3}$$

is the polarization induced by $\mathbf{E}(\mathbf{r}, t)$ in the *unperturbed* waveguide whose dielectric constant is $\varepsilon(\mathbf{r})$. The perturbation polarization $\mathbf{P}_{\text{pert}}(\mathbf{r}, t)$ is then defined by (13.3-2) and represents any deviation of the polarization from that of the unperturbed waveguide. Using (13.3-2) and (13.3-3) in (13.3-1) gives

$$\nabla^2 E_y - \mu\varepsilon(\mathbf{r}) \frac{\partial^2 E_y}{\partial t^2} = \mu \frac{\partial^2}{\partial t^2} [P_{\text{pert}}(\mathbf{r}, t)]_y \tag{13.3-4}$$

and similar expressions for E_x and E_z.

Ignoring the possibility of coupling to the continuum of radiation modes, regimes *d* and *e* in Figure 13-2, we expand the total field in the "perturbed" waveguide as a superposition of confined modes

$$E_y(\mathbf{r}, t) = \tfrac{1}{2} \sum_m A_m(z)\mathscr{E}_y^{(m)}(x)e^{i(\omega t - \beta_m z)} + \text{c.c.} \tag{13.3-5}$$

where m indicates the mth discrete eigenmode of (13.2-5), which satisfies

$$\left(\frac{\partial^2}{\partial x^2} - \beta_m^2\right)\mathscr{E}_y^{(m)}(\mathbf{r}) + \omega^2\mu\varepsilon(\mathbf{r})\mathscr{E}_y^{(m)}(\mathbf{r}) = 0 \tag{13.3-6}$$

where $\varepsilon(\mathbf{r}) = \varepsilon_0 n^2(\mathbf{r})$.

Substitution of (13.3-5) in (13.3-4) leads to

$$\begin{aligned} e^{i\omega t} \sum_m \Bigg[& \frac{A_m}{2} \left(-\beta_m^2 \mathscr{E}_y^{(m)} + \frac{\partial^2 \mathscr{E}_y^{(m)}}{\partial x^2} + \omega^2\mu\varepsilon(\mathbf{r})\mathscr{E}_y^{(m)} \right) e^{-i\beta_m z} \\ & + \frac{1}{2} \left(-2i\beta_m \frac{dA_m}{dz} + \frac{d^2 A_m}{dz^2} \right) \mathscr{E}_y^{(m)} e^{-i\beta_m z} \Bigg] + \text{c.c.} \\ & = \mu \frac{\partial^2}{\partial t^2} [P_{\text{pert}}(\mathbf{r}, t)]_y \end{aligned} \tag{13.3-7}$$

First we note that in view of (13.3-6) the sum of the first three terms in

(13.3-7) is zero. We assume "slow" variation so that

$$\left|\frac{d^2 A_m}{dz^2}\right| \ll \beta_m \left|\frac{dA_m}{dz}\right|$$

and obtain from (13.3-7)

$$\sum_m -i\beta_m \frac{dA_m}{dz} \mathscr{E}_y^{(m)} e^{i(\omega t - \beta_m z)} + \text{c.c.} = \mu \frac{\partial^2}{\partial t^2} [P_{\text{pert}}(\mathbf{r}, t)]_y \qquad (13.3\text{-}8)$$

We take the product of (13.3-8) with $\mathscr{E}_y^{(s)}(x)$ and integrate from $-\infty$ to ∞. The result, using (13.2-8), is

$$\frac{dA_s^{(-)}}{dz} e^{i(\omega t + \beta_s z)} - \frac{dA_s^{(+)}}{dz} e^{i(\omega t - \beta_s z)} - \text{c.c.} = -\frac{i}{2\omega} \frac{\partial^2}{\partial t^2} \int_{-\infty}^{\infty} [P_{\text{pert}}(\mathbf{r}, t)]_y \mathscr{E}_y^{(s)}(x)\, dx \qquad (13.3\text{-}9)$$

The presence of two terms on the left side of Equation (13.3-9) is due to the fact that the summation over m in (13.3-8) contains two terms involving $\mathscr{E}_y^{(m)}(x)$ for each value of m—one, designated as $(-)$, traveling in the $-z$ direction, and the other $(+)$, traveling in the $+z$ direction.

Equation 13.3-9 can be used to treat a large variety of mode interactions [12]. Each physical example involves, in general, a different perturbation polarization $\mathbf{P}_{\text{pert}}(\mathbf{r}, t)$. They all, however, lead to the same set of "coupled mode" equations of the form of Equation (13.5-1). Some important examples are considered in the following sections.

13.4 PERIODIC WAVEGUIDE

Consider a periodic dielectric waveguide in which the periodicity is due to a corrugation of one of the interfaces as shown in Figure 13-6. Such periodic waveguides are used for optical filtering [16] as well as in the distributed feedback laser [17–19]. These two applications will be described further below.

The corrugation is described by the dielectric perturbation $\Delta\varepsilon(\mathbf{r}) \equiv \varepsilon_0 \Delta n^2(\mathbf{r})$ such that the total dielectric constant is

$$\varepsilon'(\mathbf{r}) = \varepsilon(\mathbf{r}) + \Delta\varepsilon(\mathbf{r})$$

The perturbation polarization is from (13.3-2) and (13.3-3)

$$\mathbf{P}_{\text{pert}}(\mathbf{r}, t) = \Delta\varepsilon(\mathbf{r})\mathbf{E}(\mathbf{r}, t) = \Delta n^2(\mathbf{r})\varepsilon_0 \mathbf{E}(\mathbf{r}, t) \qquad (13.4\text{-}1)$$

Since $\Delta n^2(\mathbf{r})$ is a scalar, it follows, from (13.3-4), that the corrugation couples only TE to TE modes and TM to TM, but not TE to TM.

To be specific consider TE mode propagation. Using (13.3-5) in (13.4-1)

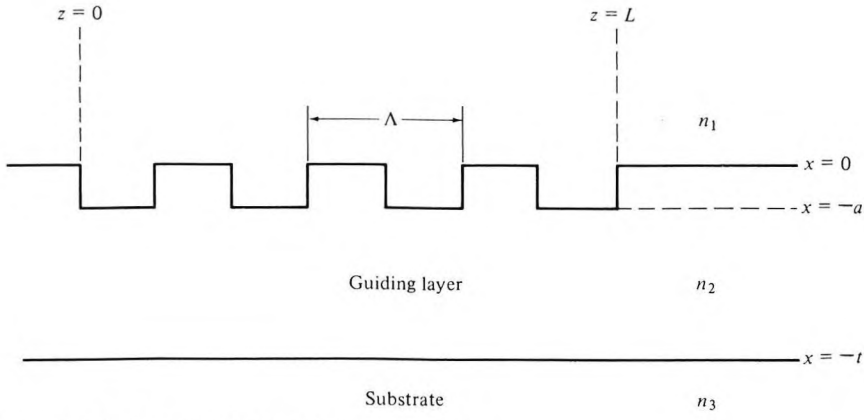

Figure 13-6 A corrugated periodic waveguide.

gives

$$[P_{\text{pert}}(\mathbf{r}, t)]_y = \frac{\Delta n^2(\mathbf{r})\varepsilon_0}{2} \sum_m [A_m \mathscr{E}_y^{(m)}(x) e^{i(\omega t - \beta_m z)} + \text{c.c.}] \qquad (13.4\text{-}2)$$

which, when used in (13.3-9), leads to

$$\frac{dA_s^{(-)}}{dz} e^{i(\omega t + \beta_s z)} - \frac{dA_s^{(+)}}{dz} e^{i(\omega t - \beta_s z)} - \text{c.c.}$$
$$= -\frac{i\varepsilon_0}{4\omega} \frac{\partial^2}{\partial t^2} \sum_m \left[A_m \int_{-\infty}^{\infty} \Delta n^2(x, z) \mathscr{E}_y^{(m)}(x) \mathscr{E}_y^{(s)}(x)\, dx e^{i(\omega t - \beta_m z)} + \text{c.c.} \right] \qquad (13.4\text{-}3)$$

We may consider the right side of (13.4-3) as a source wave term driving the forward wave $A_s^{(+)} \exp [i(\omega t - \beta_s z)]$ and the backward wave $A_s^{(-)} \exp [i(\omega t + \beta_s z)]$ on the left side. In order for a wave to be driven by a source, both source wave and driven wave must have the same frequency so that the interaction will not average out to zero over a long time (long compared to a period of their difference frequency). Equally important: Both source and wave need to have nearly the same phase dependence $\exp (i\beta z)$ so that the interaction does not average out to zero with distance of propagation z. If, for example, it is desired that the forward wave $A_s^{(+)} \exp [i(\omega t - \beta_s z]$ be excited, it is necessary that at least one term on the right side of (13.4-3), say the lth one, vary as $\exp [i(\omega t - \beta z)]$ with $\beta \approx \beta_s$. If no other terms on the right side of (13.4-3) satisfy this condition, we simplify the equation by keeping only the forward wave on the left side and the lth on the right. We describe this situation by saying that the perturbation $\Delta n^2(x, z)$ couples the forward $(+s)$ mode to the lth mode and vice versa.

To be specific, let us assume that the period Λ in the z direction of the perturbation $\Delta n^2(x, z)$ is so chosen that $\ell\pi/\Lambda \approx \beta_s$ for some integer l. We

can expand $\Delta n^2(x, z)$ of a square wave perturbation as a Fourier series

$$\Delta n^2(x, z) = \Delta n^2(x) \sum_{-\infty}^{\infty} a_q e^{i(2q\pi/\Lambda)z} \tag{13.4-4}$$

The right side of (13.4-3) now contains a term ($q = l$, $m = s$) proportional to $A_s^{(+)} \exp [i(2l\pi/\Lambda - \beta_s)z]$. But

$$\frac{2l\pi}{\Lambda} - \beta_s \approx \beta_s$$

so that this term is capable of driving synchronously the amplitude $A_s^{(-)} \exp (i\beta_s z)$ on the left side of (13.4-3) with the result

$$\frac{dA_s^{(-)}}{dz} = \frac{i\omega\varepsilon_0}{4} A_s^{(+)} \int_{-\infty}^{\infty} \Delta n^2(x)[\mathscr{E}_y^{(s)}(x)]^2 \, dx a_l e^{i[(2l\pi/\Lambda)-2\beta_s]z} \tag{13.4-5}$$

The coupling between the backward $A_s^{(-)}$ and the forward $A_s^{(+)}$ by the lth harmonic of $\Delta n^2(x, z)$ can thus be described by

$$\frac{dA_s^{(-)}}{dz} = \kappa A_s^{(+)} e^{-i2(\Delta\beta)z} \tag{13.4-6}$$

and reciprocally

$$\frac{dA_s^{(+)}}{dz} = \kappa^* A_s^{(-)} e^{i2(\Delta\beta)z}$$

where

$$\kappa = \frac{i\omega\varepsilon_0 a_l}{4} \int_{-\infty}^{\infty} \Delta n^2(x)[\mathscr{E}_y^{(s)}(x)]^2 \, dx \tag{13.4-7}$$

$$\Delta\beta \equiv \beta_s - \frac{l\pi}{\Lambda} \equiv \beta_s - \beta_0 \tag{13.4-8}$$

We note that the total power carried by both modes is conserved, since

$$\frac{d}{dz} [|A_s^{(-)}|^2 - |A_s^{(+)}|^2] = 0 \tag{13.4-9}$$

Let us consider the specific "square-wave" corrugation of Figure 13-6. In this case the periodicity (period = Λ) in the z direction is accounted for by taking

$$\begin{aligned} \Delta n^2(x, z) &= \Delta n^2(x) \left[\frac{1}{2} + \frac{2}{\pi}\left(\sin \eta z + \frac{1}{3} \sin 3\eta z + \cdots\right)\right] \\ &= \Delta n^2(x) \sum_l a_l e^{i\eta l z} \qquad l = 1, 3, 5, \ldots \end{aligned} \tag{13.4-10}$$

where

$$\Delta n^2(x) = \begin{cases} n_1^2 - n_2^2 & -a \le x \le 0 \\ 0 & \text{elsewhere} \end{cases} \tag{13.4-11}$$

$$\eta \equiv \frac{2\pi}{\Lambda}$$

so that

$$a_l = \begin{cases} \dfrac{-i}{\pi l} & l \text{ odd} \\ 0 & l \text{ even} \\ \frac{1}{2} & l = 0 \end{cases}$$

and for l odd we obtain from (13.4-7) and (13.4-10)

$$\kappa = \frac{+\omega\varepsilon_0}{4\pi l} \int_{-\infty}^{\infty} \Delta n^2(x)[\mathscr{E}_y^{(s)}(x)]^2 \, dx \tag{13.4-12}$$

In practice the period Λ is chosen so that, for some particular l, $\Delta\beta \approx 0$. We note that for $\Delta\beta = 0$

$$\Lambda = l\frac{\lambda_g^{(s)}}{2} \tag{13.4-13}$$

where $\lambda_g^{(s)} = 2\pi/\beta_s$ is the guide wavelength of the sth mode.

We can now use the field expansion (13.2-3) plus (13.4-11) to perform the integration of (13.4-12).

$$\begin{aligned} \int_{-\infty}^{\infty} \Delta n^2(x)[\mathscr{E}_y^{(s)}(x)]^2 \, dx &= (n_1^2 - n_2^2) \int_{-a}^{0} [\mathscr{E}_y^{(s)}(x)]^2 \, dx \\ &= (n_1^2 - n_2^2)C_s^2 \int_{-a}^{0} \left[\cos h_s x - \frac{q_s}{h_s} \sin h_s x\right]^2 dx \end{aligned} \tag{13.4-14}$$

Although the integral can be calculated exactly using (13.2-3) and (13.2-5), an especially simple result follows if we consider that operation is sufficiently above propagation cutoff, $t(n_2 - n_3)/s\lambda \gg 1$ so that from (13.2-4) and (13.2-5)

$$\begin{aligned} &\beta_s \approx n_2 k_0 \\ &h_s \to \frac{\pi s}{t} \qquad s = 1, 2, \ldots = \text{transverse mode number} \\ &\frac{q_s}{h_s} \approx (n_2^2 - n_1^2)^{1/2} \left(\frac{2t}{s\lambda}\right) \end{aligned} \tag{13.4-15}$$

The results can be verified using (13.2-4) and (13.2-5). In addition since $q_s \gg h_s$, we have, from (13.2-7),

$$C_s^2 = \frac{4h_s^2\omega\mu}{\beta_s t q_s^2} \tag{13.4-16}$$

in the well-confined regime and for $h_s a \ll 1$ the integral of (13.4-14) becomes

$$(n_1^2 - n_2^2) \int_{-a}^{0} [\mathcal{E}_y^{(s)}(x)]^2 \, dx = (n_1^2 - n_2^2) \frac{4\pi^2 \omega \mu}{3 n_2 k_0} \left(\frac{a}{t}\right)^3 s^2 \left(1 + \frac{3}{q_s a} + \frac{3}{q_s^2 a^2}\right)$$

and, using (13.4-15),

$$\kappa_s \approx \frac{2\pi^2 s^2}{3 l \lambda} \frac{(n_2^2 - n_1^2)}{n_2} \left(\frac{a}{t}\right)^3 \left[1 + \frac{3}{2\pi} \frac{\lambda/a}{(n_2^2 - n_1^2)^{1/2}} + \frac{3}{4\pi^2} \frac{(\lambda/a)^2}{(n_2^2 - n_1^2)}\right] \tag{13.4-17}$$

The problem of two-wave coupling by a corrugation has thus been reduced to a pair of coupled differential equations (13.4-6) and an expression (13.4-17) for the coupling constant.

13.5 COUPLED-MODE SOLUTIONS

Let us return to the coupled-mode equations (13.4-6). For simplicity let us put $A_s^{(-)} \equiv A$, $A_s^{(+)} \equiv B$ and write them as

$$\begin{aligned} \frac{dA}{dz} &= \kappa_{ab} B e^{-i2(\Delta\beta)z} \\ \frac{dB}{dz} &= \kappa_{ab}^* A e^{+i2(\Delta\beta)z} \end{aligned} \tag{13.5-1}$$

Consider a waveguide with a corrugated section of length L as in Figure 13-6. A wave with an amplitude $B(0)$ is incident from the left on the corrugated section.

The solution of (13.5-1) for this case subject to $A(L) = 0$ is

$$\begin{aligned} A(z)e^{i\beta z} &= B(0) \frac{i\kappa_{ab} e^{i\beta_0 z}}{-\Delta\beta \sinh SL + iS \cosh SL} \sinh [S(z - L)] \\ B(z)e^{-i\beta z} &= B(0) \frac{e^{-i\beta_0 z}}{-\Delta\beta \sinh SL + iS \cosh SL} \\ &\quad \times \{\Delta\beta \sinh [S(z - L)] + iS \cosh [S(z - L)]\} \end{aligned} \tag{13.5-2}$$

where

$$\begin{aligned} S &= \sqrt{\kappa^2 - (\Delta\beta)^2} \\ \kappa &\equiv |\kappa_{ab}| \end{aligned} \tag{13.5-3}$$

Under these matching conditions $\Delta\beta = 0$, we have

$$\begin{aligned} A(z) &= B(0) \frac{\kappa_{ab}}{\kappa} \frac{\sinh [\kappa(z - L)]}{\cosh \kappa L} \\ B(z) &= B(0) \frac{\cosh [\kappa(z - L)]}{\cosh \kappa L} \end{aligned} \tag{13.5-4}$$

A plot of the mode powers $|B(z)|^2$ and $|A(z)|^2$ for this case is shown in Figure 13-7. For sufficiently large arguments of the cosh and sinh functions

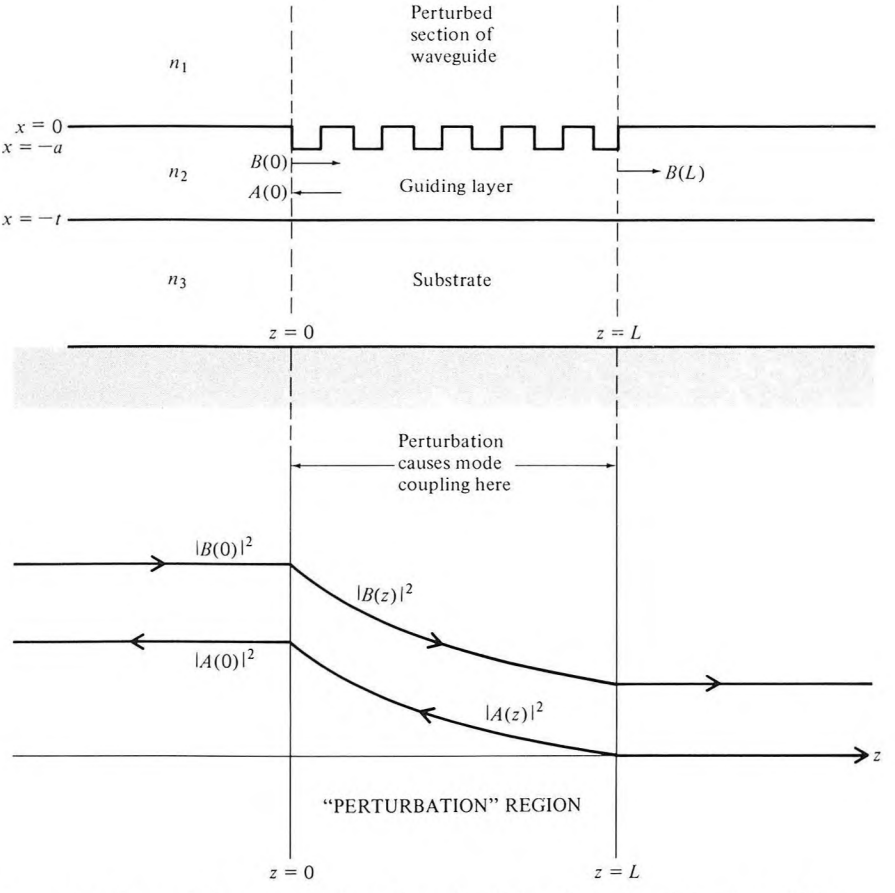

Figure 13-7 (*upper*) A corrugated section of a dielectric waveguide. (*lower*) The incident and reflected intensities inside the corrugated section.

in (13.5-4), the incident mode power drops off exponentially along the perturbation region. This behavior, however, is due not to absorption but to *reflection* of power into the backward traveling mode, A.

From (13.3-5) and (13.5-2) we find that the z dependent part of the wave solutions in the periodic waveguide are exponentials with propagation constants

$$\beta' = \beta_0 \pm iS = \frac{l\pi}{\Lambda} \pm i\sqrt{\kappa^2 - [\beta(\omega) - \beta_0]^2} \qquad \text{(13.5-5)}$$

where we used $\Delta\beta \equiv \beta - \beta_0$, $\beta_0 \equiv \pi l/\Lambda$.

We note that for a range of frequencies such that $\Delta\beta(\omega) < \kappa$, β' has an imaginary part. This is the so-called "forbidden" region in which the evanescence behavior shown in Figure 13-7 occurs and which is formally analogous to the energy gap in semiconductors where the periodic crystal potential causes the electron propagation constants to become complex. Note

that for each value of l, $l = 1, 2, 3 \ldots$, there exists a gap whose center frequency ω_{0l} satisfies $\beta(\omega_{0l}) = l\pi/\Lambda$. The exceptions are values of l for which κ is zero. We can approximate $\beta(\omega)$ near its Bragg value $(\pi l/\Lambda)$ by $\beta(\omega) \approx (\omega/c)n_{\text{eff}}$ (n_{eff} is an effective index of refraction). The result is

$$\beta' \cong \frac{l\pi}{\Lambda} \pm i\left[\kappa^2 - \left(\frac{n_{\text{eff}}}{c}\right)^2 (\omega - \omega_0)^2\right]^{1/2} \tag{13.5-6}$$

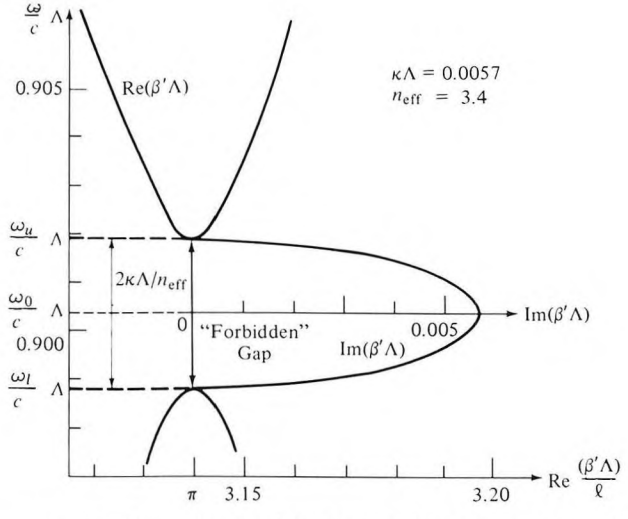

Figure 13-8 Dependence of the real and imaginary parts of the mode propagation constant, β', of the modes in a periodic waveguide. At frequencies $\omega_l < \omega < \omega_u$, $\text{Im}(\beta') \neq 0$ and the modes are evanescent. At these frequencies, Re $\beta' = l\pi/\Lambda$.

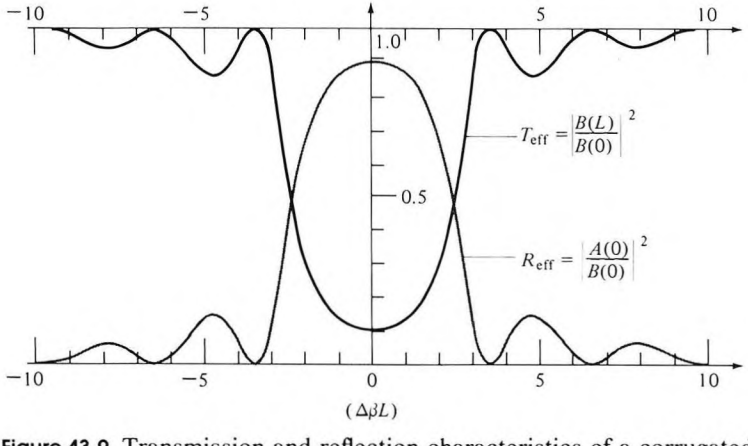

Figure 13-9 Transmission and reflection characteristics of a corrugated section of length L, as a function of the detuning $\Delta\beta L \approx [(\omega - \omega_0)L/c]n_{\text{eff}}$ ($\kappa L = 1.84$).

where ω_0, the midgap frequency, is the value of ω for which the unperturbed β is equal to $\beta_0 \equiv l\pi/\Lambda$.

A plot of Re β' and Im β' (for $l = 1$) versus ω, based on (13.5-6), is shown in Figure 13-8. We note that the height of the "forbidden" frequency zone is

$$(\Delta\omega)_{\text{gap}} = \frac{2\kappa c}{n_{\text{eff}}} \tag{13.5-7}$$

where κ is according to (13.4-17) a function of the integer l. It follows from (13.5-6) that

$$(\text{Im } \beta')_{\max} = \kappa \tag{13.5-8}$$

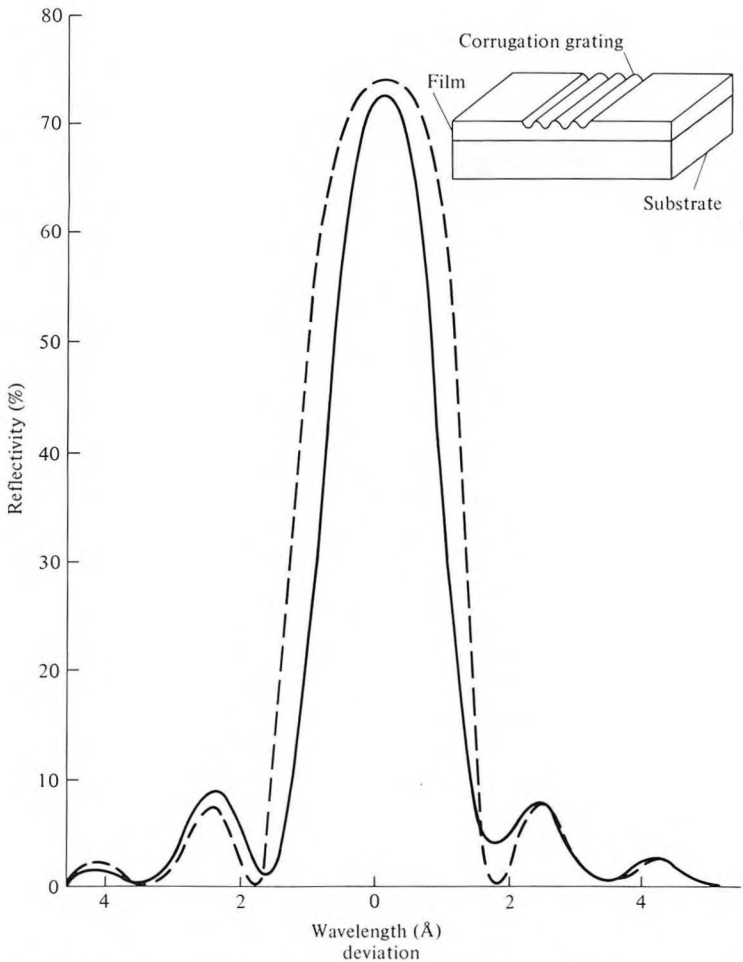

Figure 13-10 Illustration of a corrugation filter in a thin-film waveguide, plot (solid line) of reflectivity of filter versus wavelength deviation from the Bragg condition, and calculated response of filter (dotted line) $|A(0)/B(0)|^2$ using (13.5-2). (After Reference [16].)

A short section of a corrugated waveguide thus acts as a high reflectivity mirror for frequencies near the Bragg value, ω_0. The transmission

$$T_{\text{eff}} = \left| \frac{B(L)}{B(0)} \right|^2$$

and reflection

$$R_{\text{eff}} = \left| \frac{A(0)}{B(0)} \right|^2$$

of such a filter are obtainable directly from (13.5-2) and are plotted in Figure 13-9. Actual transmission characteristics of a corrugated waveguide are shown in Figure 13-10.

13.6 DISTRIBUTED FEEDBACK LASERS

If a periodic medium is provided with sufficient gain at frequencies near the Bragg frequency ω_0 where $(l\pi/\Lambda \approx \beta)$, oscillation can result without the benefit of end reflectors. The feedback is now provided by the continuous coherent backscattering from the periodic perturbation. In the following discussion we will consider two generic cases: (1) the bulk properties of a medium are perturbed periodically [17]; (2) the boundary of a waveguide laser is perturbed periodically [18]. Both cases will be found to lead to the same set of equations.

Bulk Periodicity

Consider a medium with a complex dielectric constant so that the propagation constant, k, is given by

$$k^2 = \omega^2\mu\varepsilon = \omega^2\mu(\varepsilon_r + i\varepsilon_i) = k_0^2 n^2(z)\left(1 + i\frac{2\gamma(z)}{k_0 n}\right) \qquad \text{(13.6-1)}$$

so that k_0 is the propagation constant in vacuum and (for $\gamma \ll k_0$) γ is the amplitude exponential gain constant.[2]

In a case where the index $n(z)$ and the gain $\gamma(z)$ are harmonic functions of z, we can write

$$\begin{aligned} n(z) &= n + n_1 \cos 2\beta_0 z \\ \gamma(z) &= \gamma + \gamma_1 \cos 2\beta_0 z \end{aligned} \qquad \text{(13.6-2)}$$

Using (13.6-2) in (13.6-1) and limiting ourselves to the case $n_1 \ll n$, $\gamma_1 \ll \gamma$, we obtain from (13.6-1)

[2] γ used here is thus one-half of that appearing in (5.4-22).

$$k^2(z) = k_0^2 n^2 + i2k_0 n\gamma + 4k_0 n\left(\frac{\pi n_1}{\lambda} + i\frac{\gamma_1}{2}\right)\cos 2\beta_0 z$$

The propagation constant in the unperturbed and lossless case ($\gamma_1 = 0$, $n_1 = 0$) is $\beta = k_0 n$. If, in addition, we define a constant κ by

$$\kappa = \frac{\pi n_1}{\lambda} + i\frac{\gamma_1}{2} \tag{13.6-3}$$

where λ is the vacuum wavelength, we can rewrite the expression for $k^2(z)$ as

$$k^2(z) = \beta^2 + i2\beta\gamma + 4\beta\kappa\cos(2\beta_0 z), \qquad \beta \equiv k_0 n \tag{13.6-4}$$

For a small fractional variation of k^2 per wavelength it was shown in Section 3.1 that the scalar wave equation can be written as

$$\frac{d^2E}{dz^2} + k^2(z)E = 0 \tag{13.6-5}$$

or using (13.6-4)

$$\frac{d^2E}{dz^2} + [\beta^2 + i2\beta\gamma + 4\beta\kappa\cos(2\beta_0 z)]E = 0$$

In the discussion following (13.4-3), it was pointed out that a spatially modulated parameter varying as $\cos 2\beta_0 z$ can couple a forward-traveling wave $\exp(-i\beta z)$ and a backward $\exp(i\beta z)$ wave of the same frequency provided $\beta_0 \cong \beta$. When this (Bragg) condition is nearly satisfied, it is impossible to describe the field $E(z)$ by a single traveling wave, but to a high degree of approximation we can take the total complex field amplitude as a linear superposition of both oppositely traveling waves

$$E(z) = A'(z)e^{i\beta' z} + B'(z)e^{-i\beta' z} \tag{13.6-6}$$

where β' is the propagation constant of the uncoupled ($\kappa = 0$) waves

$$\beta'^2 = \beta^2 + i2\beta\gamma$$
$$(\beta' \approx \beta + i\gamma,\ \gamma \ll \beta) \tag{13.6-7}$$

Using (13.6-6) and

$$\frac{d^2}{dz^2}(A'(z)e^{i\beta' z}) = -\left(\beta'^2 A' - 2i\beta'\frac{dA'}{dz} - \frac{d^2A'}{dz^2}\right)e^{i\beta' z}$$

in (13.6-5), assuming "slow" variation so that $d^2A'/dz^2 \ll \beta' dA'/dz$, gives

$$i\beta'\frac{dA'}{dz}e^{i\beta' z} - i\beta'\frac{dB'}{dz}e^{-i\beta' z} = -\beta\kappa e^{i(2\beta_0-\beta')z}B' - \beta\kappa e^{-i(2\beta_0-\beta')z}A'$$
$$- \beta\kappa e^{i(2\beta_0+\beta')}A' - \beta\kappa e^{-i(2\beta_0+\beta')z}B' \tag{13.6-8}$$

For operation near the Bragg condition, $\beta_0 \approx \beta$, we can separately equate terms with nearly equal phase variation (that is, synchronous), thus ignoring

the last two terms in (13.6-8). We obtain

$$\frac{dA'}{dz} = i\kappa B' e^{-i2(\beta'-\beta_0)z} = i\kappa B' e^{-i2(\Delta\beta+i\gamma)z}$$

$$\frac{dB'}{dz} = -i\kappa A' e^{+i2(\beta'-\beta_0)z} = -i\kappa A' e^{i2(\Delta\beta+i\gamma)z}$$

$$\Delta\beta \equiv \beta - \beta_0 = \frac{\omega}{c} n - \frac{\pi}{\Lambda} \qquad \Lambda = \text{period of spatial variation} \tag{13.6-9}$$

We will next derive a similar set of equations to describe a corrugated waveguide laser.

Corrugated Waveguide Laser

The case of a passive corrugated waveguide is described by (13.5-1). If the guiding medium possesses gain we simply need to modify these equations by adding gain terms so that when $\kappa = 0$ the two independent solutions, $A(z)$ and $B(z)$, correspond to exponentially growing waves along the $-z$ and the $+z$ directions, respectively. We thus replace (13.5-1) by

$$\frac{dA}{dz} = \kappa_{ab} B e^{-i2(\Delta\beta)z} - \gamma A$$

$$\frac{dB}{dz} = \kappa_{ab}^* A e^{i2(\Delta\beta)z} + \gamma B \tag{13.6-10}$$

where κ is given by (13.4-12) and γ is the exponential gain constant of the medium. Defining $A'(z)$ and $B'(z)$ by

$$A(z) = A'(z)e^{-\gamma z}$$
$$B(z) = B'(z)e^{\gamma z} \tag{13.6-11}$$

Equations 13.6-10 become

$$\frac{dA'}{dz} = \kappa_{ab} B' e^{-i2(\Delta\beta+i\gamma)z}$$

$$\frac{dB'}{dz} = \kappa_{ab}^* A' e^{+i2(\Delta\beta+i\gamma)z} \tag{13.6-12}$$

and are thus in a form identical to that of (13.6-9) derived for the case of a bulk periodic medium with index modulation.

Equations 13.6-12 become identical to (13.5-1) provided we replace

$$\Delta\beta \longrightarrow \Delta\beta + i\gamma \tag{13.6-13}$$

With this substitution we can then use (13.5-2) to write directly the solutions for the incident wave, $E_i = B'(z)\exp[(-i\beta + \gamma)z]$, and the reflected wave

$E_r = A(z)e^{i\beta z} = A'(z)^{[i\beta-\gamma]z}$, within a section of length L in the case of a single mode with amplitude $B(0)$ incident on the corrugated section at $z = 0$.

$$E_i(z) = B(0)\frac{e^{-i\beta_0 z}\{(\gamma - i\Delta\beta)\sinh[S(L-z)] - S\cosh[S(L-z)]\}}{(\gamma - i\Delta\beta)\sinh SL - S\cosh SL}$$

$$E_r(z) = B(0)\frac{\kappa_{ab}e^{i\beta_0 z}\sinh[S(L-z)]}{(\gamma - i\Delta\beta)\sinh SL - S\cosh SL} \tag{13.6-14}$$

where

$$S^2 = \kappa^2 + (\gamma - i\Delta\beta)^2 \tag{13.6-14a}$$

The fact that S now is complex makes for a qualitative difference between the behavior of the passive periodic guide (13.5-2) and the periodic guide with gain (13.6-14). To demonstrate this difference consider the case when the condition

$$(\gamma - i\Delta\beta)\sinh SL = S\cosh SL \tag{13.6-15}$$

is satisfied. It follows from (13.6-14) that both the reflectance, $E_r(0)/E_i(0)$, and the transmittance, $E_i(L)/E_i(0)$, become infinite. The device acts as an oscillator, since it yields finite output fields $E_r(0)$ and $E_i(L)$ with no input $[E_i(0) = 0]$. Condition (13.6-15) is thus the oscillation condition for a distributed feedback laser [17]. For the case of $\gamma = 0$ it follows, from (13.5-2), that $|E_i(L)/E_i(0)| < 1$ and $|E_r(0)/E_i(0)| < 1$ as appropriate to a passive device with no internal gain.

For frequencies very near the Bragg frequency $\omega_0(\Delta\beta \cong 0)$ and for sufficiently high gain constant γ so that (13.6-15) is nearly satisfied, the guide acts as a high gain amplifier. The amplified output is available either in reflection with a ("voltage") gain

$$\frac{E_r(0)}{E_i(0)} = \frac{\kappa_{ab}\sinh SL}{(\gamma - i\Delta\beta)\sinh SL - S\cosh SL} \tag{13.6-16}$$

or in transmission with a gain

$$\frac{E_i(L)}{E_i(0)} = \frac{-Se^{-i\beta_0 L}}{(\gamma - i\Delta\beta)\sinh SL - S\cosh SL} \tag{13.6-17}$$

The behavior of the incident and reflected field for a high gain case is sketched in Figure 13-11. Note the qualitative difference between this case and the passive one depicted in Figure 13-7.

The reflection gain, $|E_r(0)/E_i(0)|^2$, and the transmission gain, $|E_i(L)/E_i(0)|^2$, are plotted in Figures 13-12 and 13-13, respectively, as a function of $\Delta\beta$ and γ. Each plot contains four infinite gain singularities at which the oscillation condition (13.6-15) is satisfied. These are four longitudinal laser modes. Higher orders exist but are not shown.

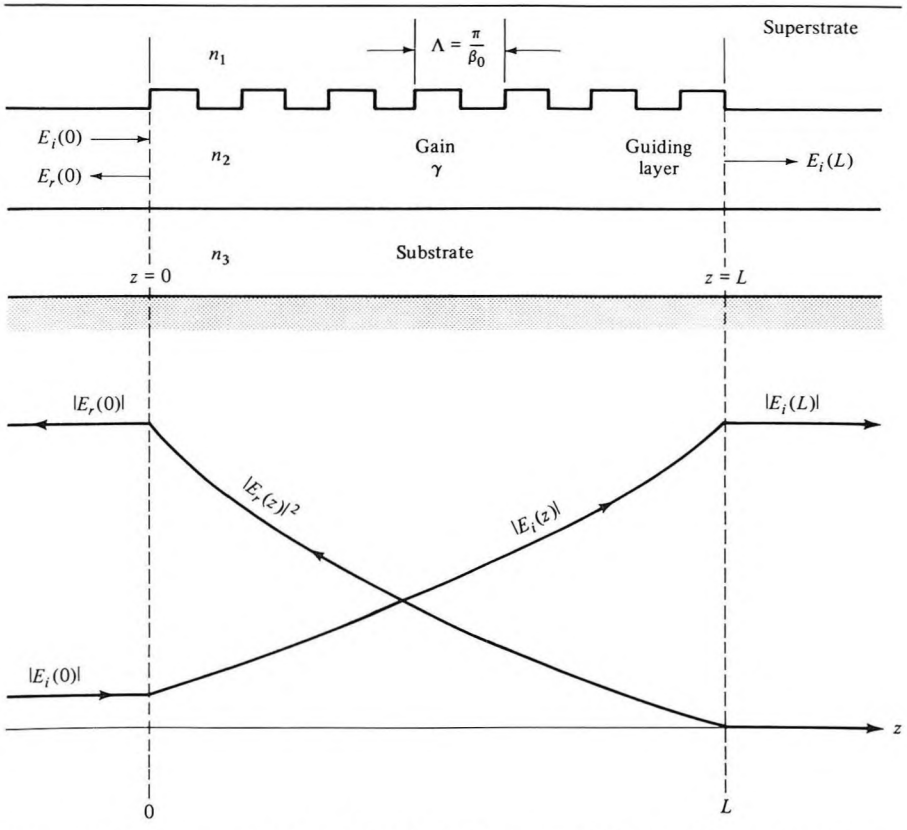

Figure 13-11 Incident and reflected fields inside an amplifying periodic waveguide.

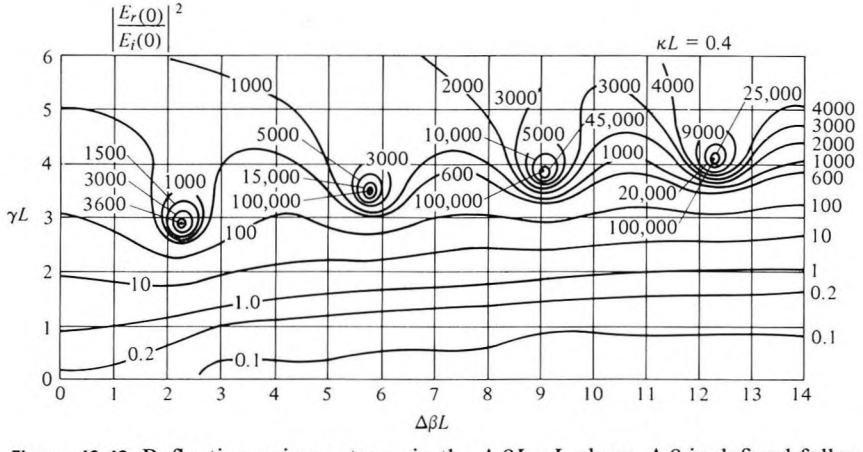

Figure 13-12 Reflection gain contours in the $\Delta\beta L$-γL plane. $\Delta\beta$ is defined following (13.6-9) and is proportional to the deviation of the frequency ω from the Bragg value $\omega_0 \equiv \pi c/\Lambda n$.

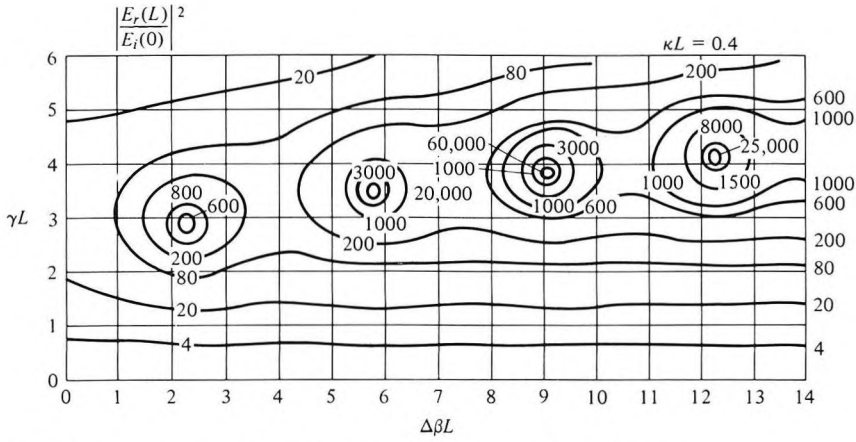

Figure 13-13 Transmission gain contours in the $\Delta\beta L$-γL plane.

Oscillation Condition

The oscillation condition (13.6-15) can be written

$$\frac{S - (\gamma - i\Delta\beta)}{S + (\gamma - i\Delta\beta)} e^{2SL} = -1 \tag{13.6-18}$$

In general, one has to resort to a numerical solution to obtain the threshold values of $\Delta\beta$ and γ for oscillation [17]. In some limiting cases, however, we can obtain approximate solutions. In the high-gain $\gamma \gg \kappa$ case we have from the definition of $S^2 = \kappa^2 + (\gamma - i\Delta\beta)^2$

$$S \approx -(\gamma - i\Delta\beta)\left(1 + \frac{\kappa^2}{2(\gamma - i\Delta\beta)^2}\right) \qquad \gamma \gg \kappa$$

so that

$$S - (\gamma - i\Delta\beta) \cong -2(\gamma - i\Delta\beta)$$

$$S + (\gamma - i\Delta\beta) \cong \frac{-\kappa^2}{2(\gamma - i\Delta\beta)}$$

and (13.6-18) becomes

$$\frac{4(\gamma - i\Delta\beta)^2}{\kappa^2} e^{2SL} = -1 \tag{13.6-19}$$

Equating the phases on both sides of (13.6-19) results in

$$2\tan^{-1}\frac{(\Delta\beta)_m}{\gamma_m} - 2(\Delta\beta)_m L + \frac{(\Delta\beta)_m L\kappa^2}{\gamma_m^2 + (\Delta\beta)_m^2} = (2m + 1)\pi$$

$$m = 0, \pm 1, \pm 2, \ldots \tag{13.6-20}$$

In the limit $\gamma_m \gg (\Delta\beta)_m, \kappa$, the oscillating mode frequencies are given by

$$(\Delta\beta_m)L \cong -\left(m + \frac{1}{2}\right)\pi \tag{13.6-21}$$

and since $\Delta\beta \equiv \beta - \beta_0 \approx (\omega - \omega_0)n_{\text{eff}}/c$

$$\omega_m = \omega_0 - \left(m + \frac{1}{2}\right)\frac{\pi c}{n_{\text{eff}}L} \tag{13.6-22}$$

We note that no oscillation can take place exactly at the Bragg frequency ω_0. The mode frequency spacing is

$$\omega_{m-1} - \omega_m \simeq \frac{\pi c}{n_{\text{eff}}L} \tag{13.6-23}$$

which is approximately the same as in a two-reflector resonator of length L.

The threshold gain value γ_m is obtained from the amplitude equality in (13.6-19)

$$\frac{e^{2\gamma_m L}}{\gamma_m^2 + (\Delta\beta)_m^2} = \frac{4}{\kappa^2} \tag{13.6-24}$$

indicating an increase in threshold with increasing mode number m. This is also evident from the numerical gain plots (Figures 13-12 and 13-13). An important feature that follows from (13.6-24) is that the threshold gain for modes with the same $|\omega - \omega_0|$, or equivalently the same $|\Delta\beta|$, is the same. Thus two modes will exist with the lowest threshold, one on each side of ω_0. This property of DFB lasers is usually undesirable, and methods for obtaining single-mode operation are discussed in the last part of this section.[3]

A diagram of a distributed feedback laser using a GaAs–GaAlAs structure is shown in Figure 13-14. The waveguiding layer as well as that providing the gain (active layer) is that of p-GaAs. The feedback is provided by corrugating the interface between the p-$Ga_{.93}Al_{.07}As$ and p-$Ga_{.7}Al_{.3}As$, where the main index discontinuity responsible for the guiding occurs.

The increase in threshold gain with the longitudinal mode index m predicted by (13.6-24) and by the plots of Figures 13-12 and 13-13 manifests itself in a high degree of mode discrimination in the distributed feedback laser.

A result that, at first, seems surprising is that there exists no laser oscillation at the Bragg frequency ω_0, that is, with $\Delta\beta = 0$. As a matter of fact, it follows from (13.6-22) and (13.6-24) that the two lowest threshold

[3] High speed (data rate) optical communication requires that the optical source put out a single frequency.

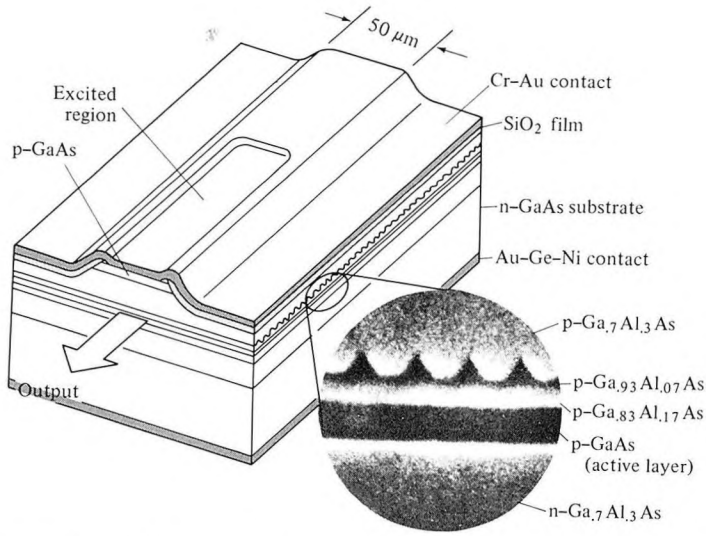

Figure 13-14 A GaAs–GaAlAs *cw* injection laser with a corrugated interface. The insert shows a scanning electron microscope photograph of the layered structure. The feedback is in third order ($l = 3$) and is provided by a corrugation with a period $\Lambda = 3\lambda_g/2 = 0.345$ μm. The thin (0.2 μm) p-$Ga_{.83}A_{.17}As$ layer provides a potential barrier which confines the injected electrons to the active (p-GaAs) layer, thus increasing the gain. (After Reference [19].)

modes are those with $m = 0$ and $m = -1$ and that they are situated symmetrically on either side of the Bragg frequency ω_0 just outside the bandgap.

To understand why the basic DFB laser of Figure 13-11 does not oscillate at the Bragg frequency, consider Figure 13-15(a). Let the reflection coefficient of a wave (at ω) incident from the left on the plane $z = 0$ be r_2 and for a wave incident from the right r_1. The reflectivity r_1, for example, is given by (13.6-16) as

$$r_1 = \frac{\kappa_{ab} \sinh SL_2}{(\gamma - i\Delta\beta) \sinh SL_2 - S \cosh SL_2}$$

$$S = \sqrt{\kappa^2 + (\gamma - i\Delta\beta)^2}$$

$$\Delta\beta = \frac{\omega}{c} n - \frac{\pi}{\Lambda} = (\omega - \omega_0) \frac{n}{c} \qquad \text{(13.6-25)}$$

where n is the modal index of refraction near ω and $\omega_0 = \pi c/n\Lambda$ is the Bragg frequency. It is obvious from the definition of r_1 and r_2 that the laser oscillation condition can be written as

$$r_1(\omega)r_2(\omega) = 1 \qquad \text{(13.6-26)}$$

which can be viewed as a condition that a wave launched at $z = 0$ in one

direction return to the starting plane after one "round trip" with the same *amplitude* and the same *phase* (modulo $m2\pi$). At $\omega = \omega_0$ the parameter S in (13.6-25) is a real number so that since $\Delta\beta = 0$, $r_{1,2} = \kappa_{ab}$ multiplied by a real number. The phase of κ_{ab} can be determined from Equations (13.4-10, 13.4-11, 13.4-12). For our choice of the plane $z = 0$ in Figure 13-15(a), the first term in the Fourier expansion (13.4-10)[4] is

$$\Delta n^2(z) = (n_1^2 - n_2^2) \sum_{\ell} a_\ell e^{i\ell(2\pi/\Lambda)z} = (n_1^2 - n_2^2) \cos \frac{2\pi}{\Lambda} z \qquad \text{(13.6-27)}$$

[4]Note that in Figure 13-6 and in the treatment of Section 13.4 we chose a plane $z = 0$ as a plane of antisymmetry. Our present choice of $z = 0$ as the plane of symmetry merely simplifies the proof and is not essential.

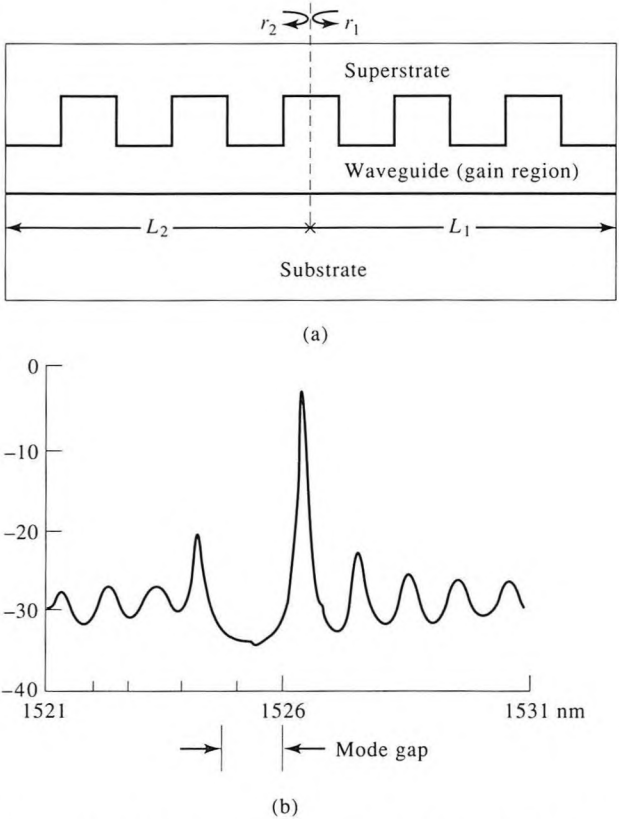

Figure 13-15 A periodic waveguide model used to derive Equation (13.6-26). (a) A periodic (DFB) waveguide laser. (b) The spontaneous emission spectrum below, but near, threshold of a DFB laser showing the mode gap. (c) A DFB laser with a phase shift section. (d) A "quarter wavelength shifted" DFB laser. (e) The spontaneous emission spectrum below threshold of a $\lambda/4$-shifted DFB laser. (Courtesy of P. C. Chen, ORTEL Corporation)

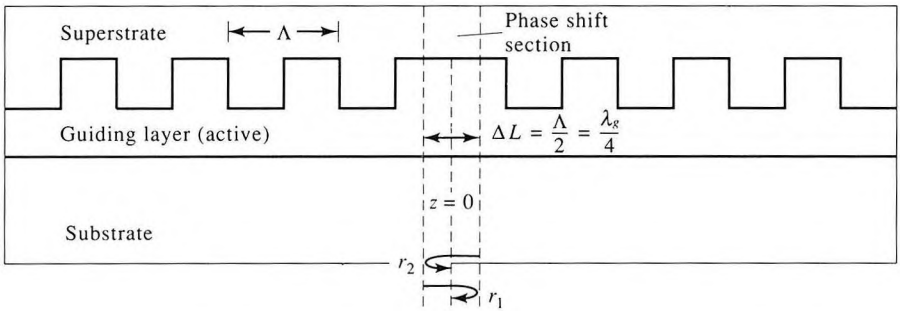
Superstrate
Λ
Phase shift section
Guiding layer (active)
ΔL = Λ/2 = λg/4
z = 0
Substrate
r2
r1

(c)

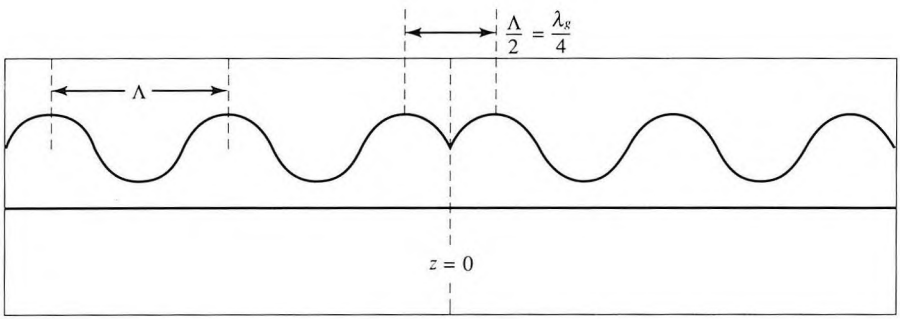
Λ/2 = λg/4
Λ
z = 0

(d)

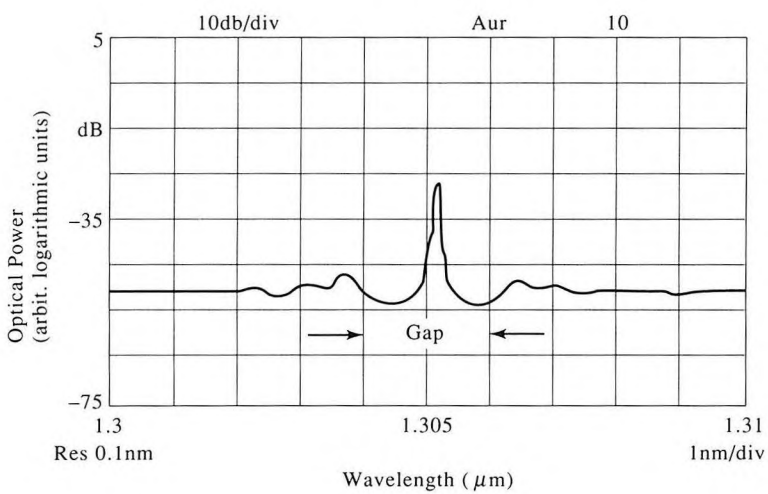
10db/div
Aur
10
5
dB
−35
−75
Optical Power
(arbit. logarithmic units)
Gap
1.3
Res 0.1nm
1.305
1.31
1nm/div
Wavelength (μm)

(e)

so that

$$a_1 = a_{-1} = \tfrac{1}{2}$$

and

$$\kappa_{ab} = i\,\frac{\omega\epsilon_0}{8}\int_{-\infty}^{\infty}(n_1^2 - n_2^2)[E_y^{(1)}(x)]^2\,dx \tag{13.6-28}$$

We thus obtain

$$r_1(\omega_0) = r_2(\omega_0) = i \times \text{some real number}$$

The product $r_1(\omega_0)r_2(\omega_0)$ is a negative number so that, according to (13.6-26), no modes exist and no oscillation can take place at the Bragg frequency ω_0. This subtle theoretical point is corroborated by the form of the spontaneous emission spectrum of a DFB laser just below oscillation threshold. Such a spectrum is shown in Figure 13-15(b). The excited DFB modes can be seen on both sides of the forbidden gap that is centered at 15,253 Å.

The lack of a single preferred oscillation mode cannot be tolerated in lasers that are used in long-haul, high-data-rate fiber communication. The existence of more than one frequency in these systems gives rise to severe pulse broadening in transmission through a long fiber [22] (see discussion in Section 2.9) and thus to a reduced data rate. One method of enabling the laser to oscillate at ω_0, and only at ω_0, is to change the phase of the reflection coefficients $r_1(\omega_0)$ and $r_2(\omega_0)$ at $z = 0$, each, by $\pi/2$ (or $-\pi/2$) so that the product $r_1(\omega_0)r_2(\omega_0)$ becomes a real number. The simplest way to achieve this is to add a uniform section of length $\Delta L = \Lambda/2 = \lambda_g/4$ [20] where $\lambda_g = 2\pi/\beta$ is the "guide" wavelength. This is shown in Figure 13.15(c). The expression for the reflection coefficient $r_1(\omega)$ [and $r_2(\omega)$] referred to the new midplane $z = 0$ is given by multiplying (13.6-25) by the additional round-trip delay factor $\exp(-i\beta\Delta L) = \exp(-i\pi/2)$. This causes the reflectances $r_{1,2}(\omega_0)$ to become real numbers so that condition (13.6-26) can be satisfied and oscillation at ω_0 is possible.

Another approach is to change the phase of κ_{ab}. If the phase of κ_{ab} is zero or π, then, according to (13.6-25), $r_1(\omega_0)$ is a real number and oscillation can take place at ω_0. This can be achieved by skipping half a period of the corrugation as shown in Figure 13-15(d). The fundamental harmonic of the corrugation can be written in this case as

$$\begin{aligned}\Delta n^2(z) &= (n_1^2 - n_2^2)\sin\left(\frac{2\pi}{\Lambda}z\right)\\ &= (n_1^2 - n_2^2)\left[\frac{-i}{2}e^{i(2\pi/\Lambda)z} + \frac{i}{2}e^{-i(2\pi/\Lambda)z}\right]\end{aligned} \tag{13.6-29}$$

The extra (i) factor in $\Delta n^2(z)$, compared to (13.6-27), causes κ_{ab} to become a real number as required.

A comparison of Figure 13-15(c) and 13-15(d) shows that conceptually these two methods are similar although we were led to them from somewhat

different points of views. The commercial DFB lasers that employ this method are called "quarter-wave shifted" DFB lasers.

Figure 13-15(e) shows the spontaneous emission spectrum below threshold of a "$\lambda/4$-shifted" [as in Figure 13-15(d)] GaInAsP 1.3 μm laser. Note the existence of a single mode at the center of the grating "forbidden" gap.

13.7 ELECTROOPTIC MODULATION AND MODE COUPLING IN DIELECTRIC WAVEGUIDES

One of the most important applications of thin film waveguiding is in optical modulation and switching. The reason is twofold: (1) The confinement of the optical radiation to dimensions comparable to λ makes it possible to achieve the magnitude of electric fields that is necessary for modulation (see Section 9.5) with relatively small applied voltages. This leads to smaller modulation powers. (2) The absence of diffraction in a guided optical beam makes it possible to use longer modulation paths (see discussion in Section 14.1).

The main principle of electrooptic modulation in dielectric waveguides involves the diversion of all or part of the power from an input TE (or TM) mode to an output TM (or TE) mode that is caused by an applied dc (that is, low-frequency) field. To be specific we consider next the case of TM $\rightarrow$ TE mode conversion. This coupling is due to a perturbation polarization[5]

$$[P_{\text{pert}}(t)]_y \propto rE^{(0)}E_x^{(\omega)}(x)e^{i\omega t} \tag{13.7-1}$$

caused by the TM mode at ω whose field is $E_x^{(\omega)}(x)$ in the presence of the dc field $E^{(0)}$. The symbol r is an appropriate linear combination of electrooptic coefficients, which will be discussed below. This polarization, acting as a source, can excite, according to (13.3-9), a TE wave $A_s^{(+)}$. The application of a dc field thus causes a TM $\rightarrow$ TE power transfer.

The complex amplitude of the y polarization at ω produced by the TM field

$$E_x^{(\omega)}(x)e^{i(\omega t-\beta_{\text{TM}}z)} \tag{13.7-2}$$

in the presence of a dc field $E^{(0)}$ is[6]

$$[P_{\text{pert}}^{(\omega)}]_y = -\frac{\varepsilon^2 rE^{(0)}}{\varepsilon_0}E_x^{(\omega)}(x)e^{-i\beta_{\text{TM}}z} \tag{13.7-3}$$

---

[5]This follows from the wave equation (13.3-1) or (13.3-9), according to which a TE mode with a field E_y can be excited by P_y. An input TM mode with a field E_x can thus excite the TE wave ($E_y \neq 0$) if the medium has an off-diagonal ε_{yx} dielectric tensor component that generates $P_y = \varepsilon_{yx}E_x$. In the electrooptic case ε_{yx} is induced by and is proportional to the applied dc field $E^{(0)}$ as in (13.7-1).

[6]The origin of relation (13.7-3) is as follows: From the basic definition of the electrooptic tensor elements $(1/n^2)_{ij}$ in (1.4-1) and from (1.4-9), it follows that a change in the indicatrix constant

Using (13.2-9) we take the TM input field $E_x^{(\omega)}(x)\exp[i(\omega t - \beta_{\mathrm{TM}} z)]$ as that of the lth mode

$$E_x^l(\mathbf{r}, t) = \frac{\beta_l}{2\omega\varepsilon(x)} B_l \mathcal{H}_y^{(l)}(x) e^{i(\omega t - \beta_l z)} + \text{c.c.} \tag{13.7-4}$$

where $\mathcal{H}_y^{(l)}(x)$ is given by (13.2-10) and $|B_l|^2$ is the mode power per unit width in the y direction. The polarization (13.7-3) can thus be written as

$$[P_{\text{pert}}(\mathbf{r}, t)]_y = -\frac{\varepsilon(x) r(x, z) E^{(0)}}{2\omega\varepsilon_0} \beta_l B_l \mathcal{H}_y^{(l)}(x) e^{i(\omega t - \beta_l z)} + \text{c.c.} \tag{13.7-5}$$

Substitution of (13.7-5) into the wave equation (13.3-9) leads to

$$\frac{dA_m^{(+)}}{dz} \exp(-i\beta_m^{\mathrm{TE}} z) - \frac{dA_m^{(-)}}{dz} \exp(i\beta_m^{\mathrm{TE}} z) = -\frac{i}{4} \int_{-\infty}^{\infty} \frac{\varepsilon(x) r(x, z) E^{(0)}(x, z)}{\varepsilon_0} \beta_l B_l \mathcal{H}_y^{(l)}(x) \mathcal{E}_y^{(m)}(x)\, dx \exp(-i\beta_l^{\mathrm{TM}} z) \tag{13.7-6}$$

If $\beta_l^{\mathrm{TM}} \approx \beta_m^{\mathrm{TE}}$, the coupling excites only the $A_m^{(+)}$ wave, that is, it is codirectional. Dropping the plus and minus superscripts we can rewrite (13.7-6) as

$$\frac{dA_m}{dz} = -i\kappa_{ml}(z) B_l e^{-i(\beta_l^{\mathrm{TM}} - \beta_m^{\mathrm{TE}})z} \tag{13.7-7}$$

$$\kappa_{ml} = \frac{\beta_l}{4} \int_{-\infty}^{\infty} \frac{\varepsilon(x) r(x, z) E^{(0)}(x, z)}{\varepsilon_0} \mathcal{H}_y^{(l)}(x) \mathcal{E}_y^{(m)}(x)\, dx \tag{13.7-8}$$

Equation (13.7-8) is general enough to apply to a large variety of cases. The dependence of $E^{(0)}$ and $r(x, z)$ on x accounts for coupling by electrooptic material in the guiding or in the bounding layers. The z dependence allows

---

$(1/n^2)_{ij}$ is related to the corresponding change in the elements of the dielectric tensor ε_{ij} by

$$\Delta\varepsilon_{ij} = -\frac{\varepsilon_{ii}\varepsilon_{jj}}{\varepsilon_0} \Delta\left(\frac{1}{n^2}\right)_{ij}$$

Using (9.1-3) we thus relate $\Delta\varepsilon_{ij}$ to an applied dc field $E_k^{(0)}$ by

$$\Delta\varepsilon_{ij} = -\frac{\varepsilon_{ii}\varepsilon_{jj}}{\varepsilon_0} r_{ijk} E_k^{(0)}$$

where r_{ijk} is the electrooptic tensor and where we sum over repeated indices. From the relation $D_i = \varepsilon_{ij} E_j + P_i$ we obtain

$$[P_{\text{pert}}^{(\omega)}]_i = \Delta\varepsilon_{ij} E_j^{(\omega)} = -\frac{\varepsilon_{ii}\varepsilon_{jj}}{\varepsilon_0} r_{ijk} E_k^{(0)} E_j^{(\omega)}$$

for the change in the ith component of the complex amplitude of the polarization at ω induced by an optical field with amplitude $E_j^{(\omega)}$ at ω in the presence of a dc field $E_k^{(0)}$. This last relation appears above in the form of (13.7-3) where the z and x dependence of $E_j^{(\omega)}$ are expressed explicitly and where

$$\varepsilon^2 r E^{(0)} \longrightarrow \varepsilon_{ii}\varepsilon_{jj} r_{ijk} E_k^{(0)}$$

for situations where $E^{(0)}$ or r depends on the longitudinal position. To be specific, we consider first the case where the guiding layer $-t < x < 0$ is uniformly electrooptic and where $E^{(0)}$ is uniform over the same region so that the integration in (13.7-8) is from $-t$ to 0. In that case, the overlap integral of (13.7-8) is maximum when the TE(m) and TM(l) modes are well confined and of the *same* order so that $l = m$. Under well-confined conditions, $p, q \gg h$ and the expressions (13.2-3), (13.2-7) for $\mathscr{E}_y^{(m)}(x)$, (13.2-10) and (13.2-13) for $\mathscr{H}_y^{(m)}(x)$ in the guiding layer become

$$\mathscr{E}_y^{(m)}(x) \longrightarrow \left(\frac{4\omega\mu}{t\beta_m^{\mathrm{TE}}}\right)^{1/2} \sin\frac{m\pi x}{t}$$

$$\mathscr{H}_y^{(m)}(x) \longrightarrow \left(\frac{4\omega\varepsilon_0 n_2^2}{t\beta_m^{\mathrm{TM}}}\right)^{1/2} \sin\frac{m\pi x}{t}$$

where for well-confined mode $\beta_l^{\mathrm{TM}} \simeq \beta_m^{\mathrm{TE}} \equiv \beta \approx k_0 n_2$. In this case the overlap integral in (13.7-8) becomes

$$\int_{-t}^{0} \mathscr{H}_y^{(m)}(x)\mathscr{E}_y^{(m)}(x)\,dx = \frac{4\omega\sqrt{\mu\varepsilon_2}}{t\beta}\int_{-t}^{0} \sin^2\frac{m\pi x}{t}\,dx$$

the coupling coefficient (13.7-8) achieves a maximum value of

$$\kappa \longrightarrow \frac{n_2^3 k_0 r E^{(0)}}{2} \tag{13.7-9}$$

The coupling is thus described by

$$\frac{dA_m}{dz} = -i\kappa B_m e^{-i(\beta_m^{\mathrm{TM}} - \beta_m^{\mathrm{TE}})z}$$

and (13.7-10)

$$\frac{dB_m}{dz} = -i\kappa A_m e^{i(\beta_m^{\mathrm{TM}} - \beta_m^{\mathrm{TE}})z}$$

The second equation of (13.7-10) can be obtained by a process similar to that leading to the first equation or by invoking the conservation of total power [12], which shows that the above expression for dB_m/dz is needed to satisfy

$$\frac{d}{dz}\left(|A_m|^2 + (B_m|^2\right) = 0$$

For the phase-matched condition $\beta_m^{\mathrm{TM}} = \beta_m^{\mathrm{TE}}$ the solution of (13.7-10) in the case of a single input ($B_m(0) \equiv B_0$, $A_m(0) = 0$) is

$$B_m(z) = B_0 \cos(\kappa z)$$

$$A_m(z) = -iB_0 \sin(\kappa z) \tag{13.7-11}$$

Using (13.7-9) we can show that the field length product $E^{(0)}L$ for which $\kappa L = \pi/2$, which is necessary to effect a complete TM $\leftrightarrow$ TE power transfer

in a distance L, is the same as that needed to go from "on" to "off" in the bulk modulator shown in Figure 9-4. This result applies only in the limit of tight confinement. In general the coupling coefficient κ is smaller than the value given by (13.7-9), and the $E^{(0)}L$ product needed to achieve a complete power transfer is correspondingly larger.

When $\beta_m^{\mathrm{TM}} \neq \beta_m^{\mathrm{TE}}$, the solution of (13.7-10), subject to boundary conditions $B_m(0) = B_0$, $A_m(0) = 0$, is

$$B(z) = B_0 e^{i\delta z}\left[\cos(sz) - \frac{i\delta}{s}\sin(sz)\right]$$

$$A(z) = -iB_0 e^{-i\delta z}\frac{\kappa}{s}\sin(sz) \tag{13.7-12}$$

where

$$s^2 \equiv \kappa^2 + \delta^2 \qquad 2\delta \equiv \beta_m^{\mathrm{TM}} - \beta_m^{\mathrm{TE}} = \beta^B - \beta^A \tag{13.7-13}$$

In contrast to the phase-matched case (13.7-11), the maximum fraction of the power that can be coupled from the input mode, B, to A is

$$\text{Fraction of power exchanged} = \frac{\kappa^2}{\kappa^2 + \delta^2} \tag{13.7-14}$$

and becomes negligible once $\delta \gg \kappa$.

A plot of the mode power for the phase-matched ($\delta = 0$) and $\delta \neq 0$ case is shown in Figure 13-16.

A deliberate periodic variation of $E^{(0)}(z)$ or $r(z)$, in this case, with a period $2\pi/(\beta_m^{\mathrm{TE}} - \beta_m^{\mathrm{TM}})$ can be used, according to (13.7-8), to compensate for the mismatch factor $\exp[-i(\beta_m^{\mathrm{TM}} - \beta_m^{\mathrm{TE}})z]$ in (13.7-10), thus leading again to a phase-matched operation.

Example: GaAs Thin-Film Modulator at $\lambda = 1$ μm

To appreciate the order of magnitude of the coupling, consider a case where the guiding layer is GaAs and $\lambda = 1$ μm. In this case (see Table 9-2)

$$n_2 \simeq 3.5 \qquad n^3 r \cong 60 \times 10^{-12}\ \frac{\mathrm{m}}{\mathrm{volt}}$$

Assuming an applied field $E^{(0)} = 10^6$ volt/m, we obtain, from (13.7-9),

$$\kappa = 1.88\ \mathrm{cm}^{-1}$$

$$l \equiv \frac{\pi}{2\kappa} = 0.83\ \mathrm{cm}$$

for the coupling constant and the power-exchange distance, respectively.

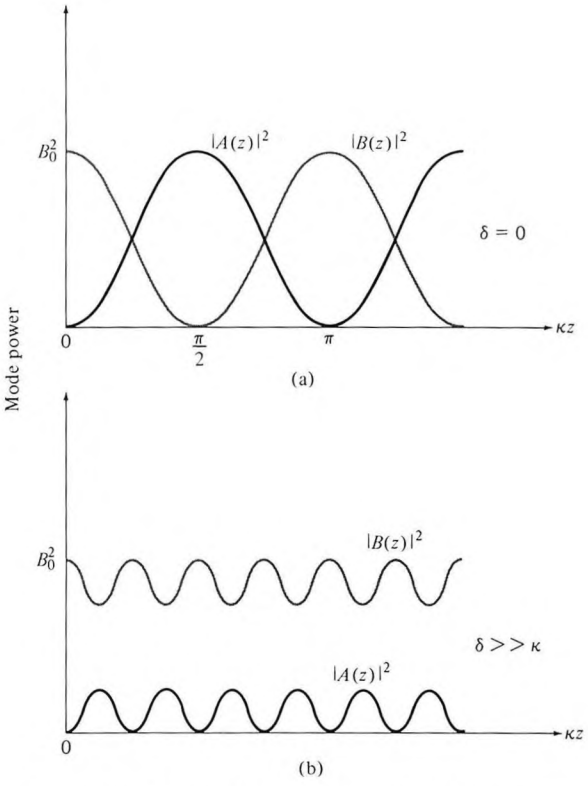

Figure 13-16 Power exchange between two coupled modes under (a) phase-matched conditions ($\beta_m^{TM} = \beta_m^{TE}$) as described by Equation (13.7-11); (b) $\beta_m^{TM} \neq \beta_m^{TE}$, Equation (13.7-12).

An experimental setup used in one of the earliest demonstrations [3] of electrooptic thin film modulation is depicted in Figure 13-17. The modulation scheme is identical to that illustrated in Figure 9-8 and depends on an electrooptic induced phase retardation (9.5-1)

$$\Gamma = (\beta_{TM} - \beta_{TE})l \approx \frac{\pi n^3 r_{41} l}{\lambda t} V \tag{13.7-15}$$

where V is the applied voltage, t and l are the height and length of the waveguide, respectively.

The ratio of the transmitted to the input intensities is given by (9.3-4), or, equivalently by (13.7-11) [note that Γ of (9.2-4) is the same as κ in (13.7-9)] as

$$\frac{I_0}{I_i} = \sin^2 \frac{\Gamma}{2} \tag{13.7-16}$$

An experimental transmission plot is shown in Figure 13-18.

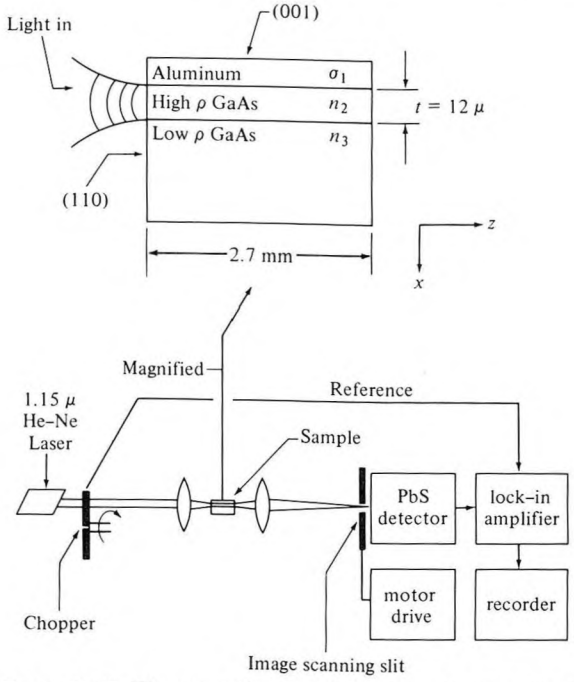

Figure 13-17 Electrooptic modulator in a GaAs epitaxial film. The modulation field is due to a reverse-bias voltage applied to the metal semiconductor junction [3].

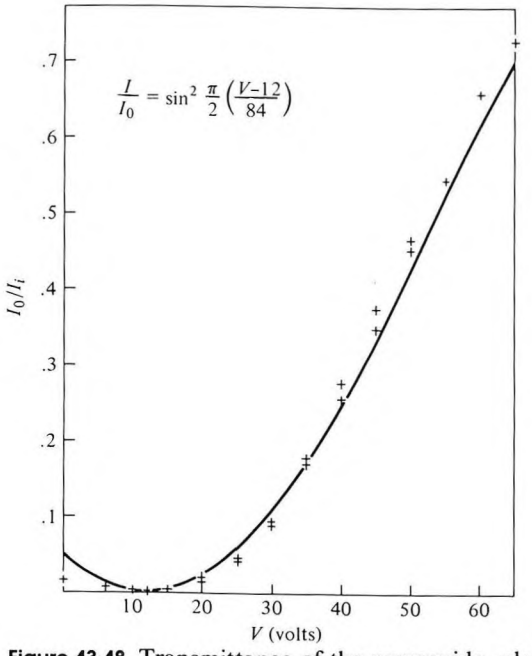

Figure 13-18 Transmittance of the waveguide, placed between crossed polarizers, as a function of the applied reverse voltage [3].

Another form of electrooptic thin film modulation utilizes two-dimensional Bragg diffraction of a waveguide mode from a spatially periodic modulation of the index of refraction. A periodic electric field set up by an interdigital electrode structure as in Figure 13-19 gives rise to the periodic variation of the index of refraction. The situation is equivalent formally to that of Bragg scattering from a sound wave, discussed in Chapter 12, where the index modulation was caused by the acoustic strain.

A necessary condition for diffraction from a mode with a propagation vector $\boldsymbol{\beta}_i$ into a mode with $\boldsymbol{\beta}_d$ is, in analogy to (12.2-1),

$$\boldsymbol{\beta}_d = \boldsymbol{\beta}_i + \mathbf{a}_G \frac{2\pi}{\Lambda} m \qquad m = 1, 2, 3, \ldots \tag{13.7-17}$$

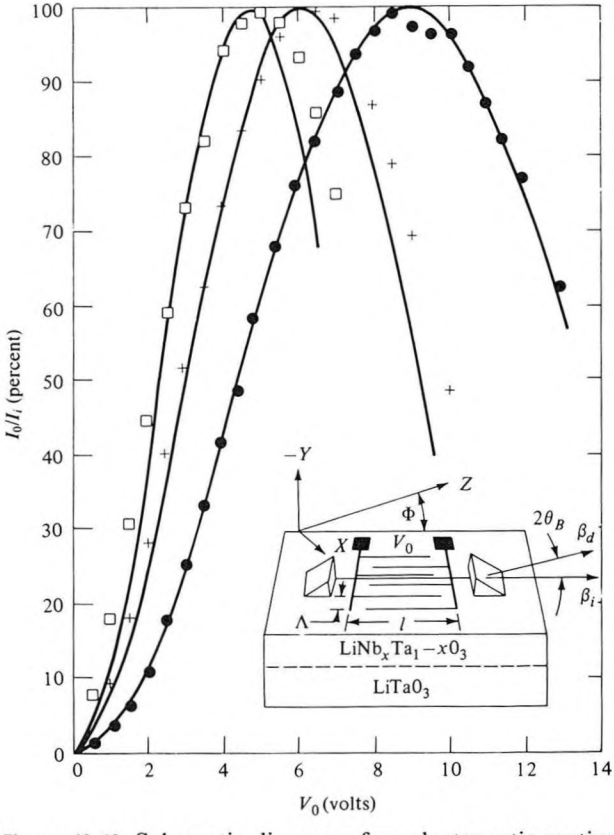

Figure 13-19 Schematic diagram of an electrooptic grating modulator in a $LiNb_xTa_{1-x}O_3$-$LiTaO_3$ waveguide. The input mode, which is coupled into the waveguide via a prism, is deflected through an angle $2\theta_B$ when a voltage is applied to the interdigital electrode structure. $\Lambda = 7.6$ μm and $l = 0.3$ cm. The curves show percentages of light diffracted as a function of voltage. Open squares 4976 Å (He–Ne laser), crosses 5598 Å (He–Ne laser), and solid circles 6328 Å (He–Ne laser). The solid curves are plots of $\sin^2(BV_0)$ normalized to the data at 75 percent. (After J. Hammer and W. Phillips, *Appl. Phys. Lett.* 24:545, 1974.)

where Λ is the period of the spatial modulation and $\mathbf{a}_G$ is a unit vector normal to the equi-index lines (that is, normal to the electrodes in Figure 13-19). The vectors $\boldsymbol{\beta}_i$ and $\boldsymbol{\beta}_d$ are in the plane of the waveguide.

The "momentum" diagram corresponding to (13.7-17) is shown in Figure 13-20 for the case of $m = 1$.

We take advantage of the formal equivalence of this case to that of Bragg diffraction from sound waves to write the diffraction efficiency, as in (12.3-16), in the form

$$\frac{I_d}{I_i} = \sin^2\left(\frac{\omega l}{2c}\Delta n\right) \tag{13.7-18}$$

where Δn is the amplitude of the index modulation and is related to the appropriate spatial Fourier component ($m = 1$ for first order Bragg diffraction), E_1 of the low-frequency electric field by (9.1-10), that is

$$\Delta n = \frac{n^3}{2} rE_1 \tag{13.7-19}$$

where r is a suitable electrooptic tensor element that depends on the crystal orientation. Combining the last two equations leads to

$$\frac{I_d}{I_i} = \sin^2\left(\frac{\pi n^3 rl}{2\lambda} E_1\right) \tag{13.7-20}$$

Since E_1 is proportional to the applied voltage V_0 the diffraction efficiency, (13.7-20) can be written as

$$\frac{I_d}{I_i} = \sin^2(BV_0) \tag{13.7-21}$$

with B inversely proportional to the optical wavelength λ.

The experimental transmission curves in Figure 13-19 are in agreement with (13.7-21).

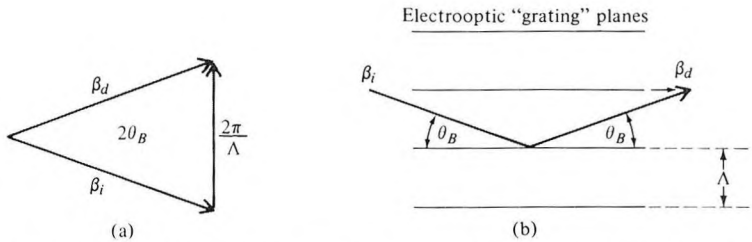

Figure 13-20 (a) A "momentum" diagram for diffraction of an input mode ($\boldsymbol{\beta}_i$) into the direction $\boldsymbol{\beta}_d$ by setting up (electrooptically) an index grating with a period Λ. (b) A top view of the waveguide plane showing the direction of the incident ($\boldsymbol{\beta}_i$), diffracted ($\boldsymbol{\beta}_d$) beams as well as the grating planes.

13.8 DIRECTIONAL COUPLING

Exchange of power between guided modes of adjacent waveguides is known as directional coupling. Waveguide directional couplers perform a number of useful functions in thin-film devices, including power division, modulation, switching, frequency selection, and polarization selection.

Waveguide coupling can be treated by the coupled-mode theory. Consider the case of the two planar waveguides illustrated in Figure 13-21. Refractive index distributions for the two guides in the absence of coupling are given by $n_a(x)$ and $n_b(x)$. The transverse electric field distribution for a particular guided mode of waveguide **a** alone and a particular mode of waveguide **b** alone will be denoted by $\mathscr{E}_y^{(a)}(x)$ and $\mathscr{E}_y^{(b)}(x)$, and their propagation constants by β_a and β_b. The field in the coupled-guide structure with an index $n_c(x)$ (for propagation in the positive z direction) is approximated by the sum of the unperturbed fields

$$E_y = A(z)\mathscr{E}_y^{(a)}(x)e^{i(\omega t-\beta_a z)} + B(z)\mathscr{E}_y^{(b)}(x)e^{i(\omega t-\beta_b z)} \tag{13.8-1}$$

In the absence of coupling—that is, if the distance between guides a and b were infinite—$A(z)$ and $B(z)$ do not depend on z and will be independent of each other, since each of the two terms on the right side of (13.8-1) satisfies the wave equation (13.3-1) separately.

The perturbation polarization responsible for the coupling is calculated by substituting (13.8-1) into (13.3-2) and (13.3-3). The result is

$$P_{\text{pert}} = e^{i\omega t}\varepsilon_0[\mathscr{E}_y^{(a)}A(z)(n_c^2(x) - n_a^2(x))e^{-i\beta_a z} + \mathscr{E}_y^{(b)}B(z)(n_c^2(x) - n_b^2(x))e^{-i\beta_b z}] \tag{13.8-2}$$

where $n_c(x)$ is the index profile of the two-guide structure. Substituting (13.8-2) in (13.3-9) and integrating over x gives

$$\frac{dA}{dz} = -i\kappa_{ab}Be^{-i(\beta_b-\beta_a)z} - iM_aA$$

$$\frac{dB}{dz} = -i\kappa_{ba}Ae^{-i(\beta_a-\beta_b)z} - iM_bB \tag{13.8-3}$$

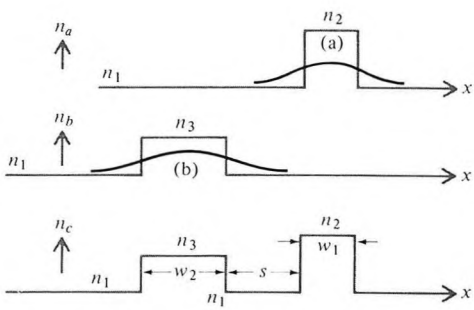

Figure 13-21 Spatial variation of the refractive index for uncoupled waveguides $n_a(x)$ and $n_b(x)$ and for a parallel waveguide structure $n_c(x)$.

where

$$\kappa_{ba}^{ab} = \frac{\omega\varepsilon_0}{4}\int_{-\infty}^{\infty}[n_c^2(x) - n_{(a,b)}^2(x)]\mathscr{E}_y^{(a)}\mathscr{E}_y^{(b)}\,dx \tag{13.8-4}$$

$$M_{(a,b)} = \frac{\omega\varepsilon_0}{4}\int_{-\infty}^{\infty}[n_c^2(x) - n_{(a,b)}^2(x)](\mathscr{E}_y^{(a,b)})^2\,dx \tag{13.8-5}$$

The terms M_a and M_b represent a small correction to the propagation constants β_a and β_b, respectively, due to the presence of the second guide. So if we take the total field as

$$E_y = A(z)\mathscr{E}_y^{(a)}e^{i[\omega t-(\beta_a+M_a)z]} + B(z)\mathscr{E}_y^{(b)}e^{i[\omega t-(\beta_b+M_b)z]}$$

instead of (13.8-1), Equations (13.8-3) become

$$\begin{aligned}\frac{dA}{dz} &= -i\kappa_{ab}Be^{-i2\delta z}\\ \frac{dB}{dz} &= -i\kappa_{ba}Ae^{i2\delta z}\end{aligned} \tag{13.8-6}$$

where

$$2\delta = (\beta_b + M_b) - (\beta_a + M_a)$$

The solution of (13.8-6) subject to a single input at guide b ($B(0) = B_0$, $A(0) = 0$) is given by (13.7-12). In terms of powers $P_a = AA^*$ and $P_b = BB^*$ in the two guides, the solution in the case $\kappa_{ba} = \kappa_{ba}$ becomes

$$\begin{aligned}P_a(z) &= P_0\frac{\kappa^2}{\kappa^2 + \delta^2}\sin^2[(\kappa^2 + \delta^2)^{1/2}z]\\ P_b(z) &= P_0 - P_a(z)\end{aligned} \tag{13.8-7}$$

where $P_0 = |B(0)|^2$ is the input power to guide b. Complete power transfer from b to a occurs in a distance $L = \pi/2\kappa$ provided $\delta = 0$ (that is, equal phase velocities in both modes). For $\delta \neq 0$, the maximum fraction of power that can be transferred is from (13.8-7)

$$\frac{\kappa^2}{\kappa^2 + \delta^2} \tag{13.8-8}$$

The coupling constant κ is given by (13.8-4). It can be evaluated straightforwardly using the field expressions (13.2-3) in the case of TE modes. In the special case of identical waveguides, $h_1 = h_2$ and $p_1 = p_2$ in Figure 13-21, one obtains

$$\kappa = \frac{2h^2pe^{-ps}}{\beta(w + 2/p)(h^2 + p^2)} \tag{13.8-9}$$

The extension to channel waveguide couplers that are confined in the y, as well as in the x, direction is straightforward. In the well-confined case

$w \gg 2/p$ and (13.8-9) simplifies to

$$\kappa = \frac{2h^2 p\, e^{-ps}}{\beta w(h^2 + p^2)} \tag{13.8-10}$$

A typical value of κ obtained at $\lambda \sim 1$ μm with w, $s \sim 3$ μm, and $\Delta n \sim 5 \times 10^{-3}$ is $\kappa \sim 5$ cm^{-1} so that coupling distances are of the order of magnitude of $\kappa^{-1} \approx 2$ mm.

A form of an electrooptic switch based on directional coupling [23] is as follows.

The length L of the coupler is chosen so that for $\delta = 0$ (that is, synchronous case) $\kappa L = \pi/2$. From (13.8-7) it follows that all the input power to guide b exits from guide a at $z = L$. The switching is achieved by applying an electric field to guide a (or b) in such a way as to change its propagation constant until

$$\delta L = \tfrac{1}{2}(\beta_a - \beta_b)L = \frac{\sqrt{3}}{2}\pi \tag{13.8-11}$$

that is, $\delta = \sqrt{3}\kappa$. It follows from (13.8-7) that at this value of δ

$$P_a = 0 \qquad P_b = P_0$$

that is, the power reappears at the output of guide b. A control of δ can thus be used to achieve any division of the powers between the outputs of guides a and b.

In practice a convenient way to control δ is to fabricate the directional coupler in an electrooptic crystal. In this case, according to (9.1-11), the application of an electric field E across one of the two waveguides will cause the index of refraction to change by

$$\Delta n \sim n^3 rE$$

where r is the appropriate electrooptic tensor element. The change Δn will give rise to a change in propagation constant

$$\delta \sim \frac{\omega}{c}\Delta n \sim \frac{\omega}{c} n^3 rE$$

The control of the power output from both arms of a directional coupler by means of an applied voltage is illustrated in Figure 13-22. The electrode geometry for applying a field to the waveguide is illustrated in Figure 13-23.

One of the interesting applications for electrooptically switched directional couplers is in the area of very high-frequency ($>5 \times 10^9$ Hz) sampling and of multiplexing and demultiplexing of optical binary pulse trains. An example of the latter is demonstrated by Figure 13-23. Two independent, but synchronized, data pulse trains A and B are fed into legs a and b, respectively, of a directional coupler. The length of the coupling section satisfies the power transfer condition $\kappa L = \pi/2$. The phase mismatch δ between the two waveguides is controlled, as discussed above, by an electric

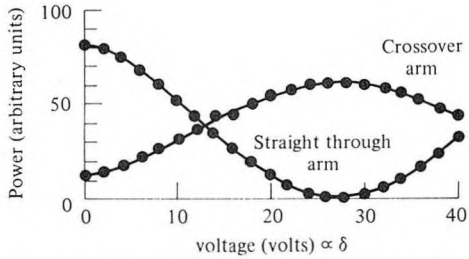

Figure 13-22 The dependence of the power output from the arms of a directional coupler as a function of the (voltage-controlled) phase constant mismatch δ. (After Reference [24].)

field applied across one of the waveguides. This electric field is due to a microwave signal at a frequency ω_m. The resulting peak phase constant mismatch, which occurs at the maxima and minima of the applied voltage, satisfies the condition (13.8-11)

$$|\delta_{\max}| = \frac{\sqrt{3}\pi}{2L} \tag{13.8-12}$$

so that the B pulses, which are synchronized to arrive during the extrema of the microwave signal, exit from arm b. Pulses A, on the other hand, arrive when the applied field, hence δ is zero, and since $\kappa L = \pi/2$, cross over and

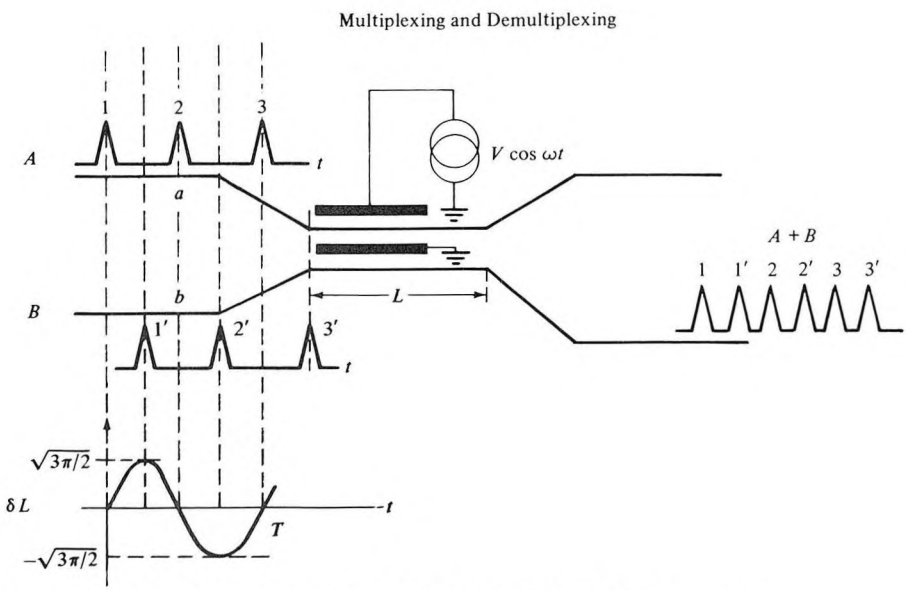

Figure 13-23 Multiplexing and demultiplexing in a directional coupling configuration.

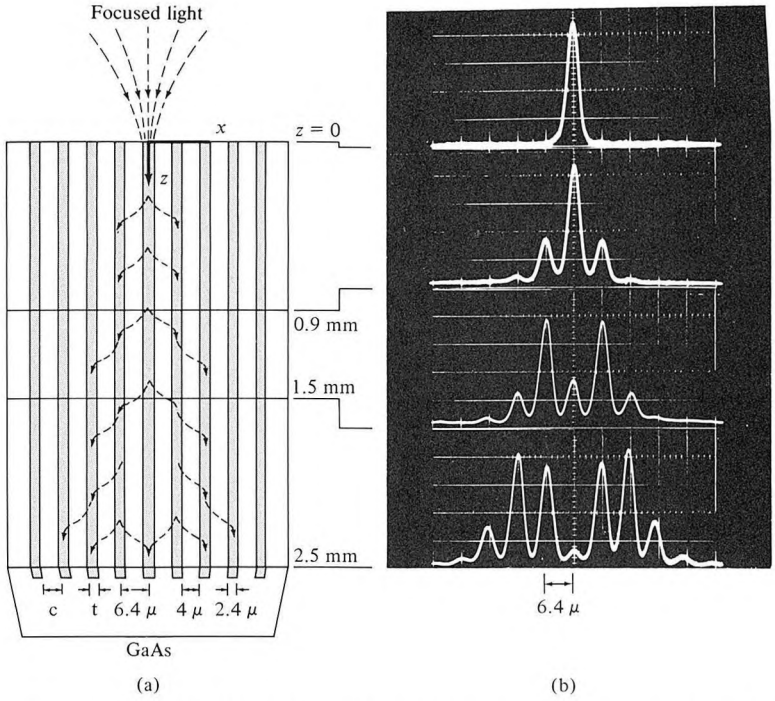

Figure 13-24 (a) Sketch of channel optical waveguide directional coupler showing flow of light energy into adjacent channels. (b) Measured guided-light intensity profiles at various lengths. The profiles have been displayed relative to the sketch at the proper value of z. Intensity scale is arbitrary. The guides were produced by proton implantation into p^+-GaAs crystal. (After Reference [23].)

exit from guide b. The result is that both pulse trains A and B are interleaved, or in the electrical engineering parlance, multiplexed in the output of guide b. The (combined) output from b can be fed into the input of a second directional coupler fed with a signal at $2\omega_m$ and multiplexed thereby with a second data train, and so on.

The device can, of course, be operated in reverse, right to left in the figure, and act as a demultiplexer for separating the dense bit train $A + B$ entering b into the individual trains A and B.

A multiguide directional coupler such as that shown in Figure 13-23 is described by a set of equations

$$\frac{dA_n}{dz} = -i\kappa A_{n-1} - i\kappa A_{n+1} \tag{13.8-13}$$

which is an obvious extension of (13.8-6) to the multimode synchronous case ($\delta = 0$) when only adjacent channels couple to each other. The solution of (13.8-13) in the case of a single input, that is, $A_n(0) = 1$, $n = 0$, $A_n(0) = 0$

$n \neq 0$ is [23]

$$A_n(z) = (-i)^n J_n(2\kappa z) \tag{13.8-14}$$

where J_n is the Bessel function of order n.

A directional coupler based on this principle is shown in Figure 13-24(a). The predicted Bessel function distribution of the intensity at various propagation distances is shown in Figure 13-24(b).

13.9 THE EIGENMODES OF A COUPLED WAVEGUIDE SYSTEM (supermodes)

In the preceding section we treated the important case of directional coupling between two parallel waveguides (Figure 13-21) by means of the coupled-mode formalism. The same problem may be approached from a different, and equivalent, point of view that is better suited for the treatment of certain important classes of experimental and device configurations. In this new point of view, we seek to obtain the propagating eigenmodes of the two-waveguide (in general, the multiwaveguide) system shown in Figure 13-21. The eigenmode is, by definition, that propagating field solution of the waveguiding structure that, except for a propagation delay factor, does not depend on the propagation coordinate z. We can obtain these mode solutions by a straightforward extension of the formalism of Section 13.1 to the more complex waveguide whose index profile $n_c(x)$ is given at the bottom of Figure 13-21. This procedure, although exact, is laborious and does not submit itself readily to the intuitive understanding that characterizes the method of solution that starts with the coupled-mode equations. The following analysis follows closely that of Reference [12].

We recall that, according to (13.8-6), the normalized, individual waveguide, mode amplitudes obey the coupled-mode equations

$$\begin{aligned} \frac{dA}{dz} &= \kappa B e^{-i2\delta z} \\ \frac{dB}{dz} &= -\kappa^* A e^{i2\delta z} \\ 2\delta &= (\beta_b - \beta_a) + (M_b - M_a) \end{aligned} \tag{13.9-1}$$

These equations are equivalent to (13.8-6) except that here $\kappa \equiv -i\kappa_{ab}$. These equations subject to boundary conditions $A(0)$ and $B(0)$ at $z = 0$ specify *a priori* (13.8-1), the total field in terms of the individual waveguides' fields.

$$\begin{aligned} a(x, z, t) &= A(z)\mathscr{E}_y^{(m)}(x)e^{i[\omega t - (\beta_a + M_a)z]} \qquad \text{in guide } a \\ b(x, z, t) &= B(z)\mathscr{E}_y^{(l)}(x)e^{i[\omega t - (\beta_b + M_b)z]} \qquad \text{in guide } b \end{aligned} \tag{13.9-2}$$

with m and l denoting the transverse mode order. Since the individual mode field profiles $\mathscr{E}_y^{(m)}(x)$ and $\mathscr{E}_y^{(l)}(x)$ are known as well as β_a, β_b, M_a, M_b, and the frequency ω, *the total field is specified once the* (*complex*) *amplitudes* $A(z)$

and $B(z)$ are given. We thus may *uniquely* describe the field at z by means of a column vector[7]

$$\mathbf{E}(z) \equiv \begin{vmatrix} B(z)e^{-i\beta_b' z} \\ A(z)e^{-i\beta_a' z} \end{vmatrix} \equiv \begin{vmatrix} E_1(z) \\ E_2(z) \end{vmatrix} \tag{13.9-3}$$

with

$$\beta_b' \equiv \beta_b + M_b$$

The evolution of $\mathbf{E}(z)$ is obtained from equations (13.9-1) as

$$\frac{d\mathbf{E}}{dz} = \tilde{\mathbf{C}}\mathbf{E} \tag{13.9-4}$$

with the matrix $\tilde{\mathbf{C}}$ given by

$$\tilde{\mathbf{C}} = \begin{vmatrix} -i\beta_b' & -\kappa^* \\ \kappa & -i\beta_a' \end{vmatrix} \tag{13.9-5}$$

Since an eigenmode depends on z only through a propagation phase factor, we postulate a solution

$$\mathbf{E}(z) = \mathbf{E}(0)e^{i\gamma z} \tag{13.9-6}$$

Combining (13.9-4) and (13.9-6) results in

$$\tilde{\mathbf{C}}\mathbf{E} = i\gamma\mathbf{E} \tag{13.9-7}$$

This is a standard matrix algebra eigenvalue problem [note similarity to Problem 2.2 and to Equation (2.1-12)], where $\mathbf{E}$ is the eigenvector and $i\gamma$ is the eigenvalue of the matrix $\tilde{\mathbf{C}}$. To determine $\mathbf{E}$ and γ, we write out the two equations represented by (13.9-7)

$$\begin{aligned} -i(\beta_b' + \gamma)E_1 - \kappa^* E_2 &= 0 \\ \kappa E_1 - i(\beta_a' + \gamma)E_2 &= 0 \end{aligned} \tag{13.9-8}$$

The condition for nontrivial solutions for E_1 and E_2 is the vanishing of the determinant of the coefficients in (13.9-8). The solution of the resulting quadratic equation yields the eigenvalues

$$\gamma_{1,2} = -\frac{\beta_a' + \beta_b'}{2} \pm \frac{1}{2}\sqrt{(\beta_a' - \beta_b')^2 + 4\kappa^2} = -\bar{\beta} \pm S \tag{13.9-9}$$

$$\bar{\beta} \equiv \frac{1}{2}(\beta_a' + \beta_b') \qquad S \equiv \sqrt{\delta^2 + \kappa^2} \qquad \kappa^2 \equiv \kappa\kappa^* \tag{13.9-10}$$

---

[7]The term *vector* is due merely to the fact that $\mathbf{E}(z)$ has two components and can thus be viewed formally as a vector in a two-dimensional space.

The two values γ_1 and γ_2 are substituted, one at a time, in (13.9-8) to obtain, to within an arbitrary constant, the corresponding eigenvectors. The result is

$$\mathbf{E}_1(z) = \begin{vmatrix} \dfrac{i\kappa^*}{\delta + S} \\ 1 \end{vmatrix} e^{-i(\bar{\beta}-S)z} \tag{13.9-11a}$$

$$\mathbf{E}_2(z) = \begin{vmatrix} \dfrac{i\kappa^*}{\delta - S} \\ 1 \end{vmatrix} e^{-i(\bar{\beta}+S)z} \tag{13.9-11b}$$

We note that, as expected, $\mathbf{E}_1 \cdot \mathbf{E}_2^* = 0$, i.e., the eigenmodes are normal. The mode norms $\mathbf{E}_2 \cdot \mathbf{E}_2^* = 1 + |\kappa|^2/(\delta \pm S)^2$ are proportional to the respective (eigen) mode powers and are thus a constant. The two components $i\kappa^*/(\delta \pm S)$ and 1 of each eigenvector represent, respectively, the normalized amplitudes of the individual waveguide modes, $\mathscr{E}_y^{(l)}(x)$ in guide b and $\mathscr{E}_y^{(m)}(x)$ in guide a, which together make up the eigenmode of the two-waveguide system. The ratio of the power in waveguides b and a in these two "supermodes" is thus $|\kappa|^2/(\delta \pm S)^2$. In the limit $\kappa/\delta \to 0$, the "velocity mismatch" limit, $\mathbf{E}_1$ and $\mathbf{E}_2$ become

$$\underset{(\kappa \ll \delta)}{\mathbf{E}_1} \to \begin{vmatrix} 0 \\ 1 \end{vmatrix} e^{-i\beta_a' z}$$

$$\underset{(\kappa \ll \delta)}{\mathbf{E}_2} \to \begin{vmatrix} 1 \\ 0 \end{vmatrix} e^{-i\beta_b' z} \tag{13.9-12}$$

to within a multiplicative constant, i.e., the super- (eigen) modes become the uncoupled single-waveguide modes.

Another important situation occurs when the two individual waveguide modes have the same phase velocity, i.e., $\delta = 0$. In this case

$$\underset{(\delta=0)}{\mathbf{E}_1(z)} = \begin{vmatrix} i\dfrac{\kappa^*}{|\kappa|} \\ 1 \end{vmatrix} e^{-i(\beta-|\kappa|)z}$$

$$\beta \equiv \beta_1 = \beta_2 \tag{13.9-13}$$

$$\underset{(\delta=0)}{\mathbf{E}_2(z)} = \begin{vmatrix} -i\dfrac{\kappa^*}{|\kappa|} \\ 1 \end{vmatrix} e^{-i(\beta+|\kappa|)z}$$

The admixture is 50–50 percent and each waveguide carries half of the total power. In the case of identical waveguides at $\delta = 0$ and for $l = m$ (i.e., same order modes), the coupling constant κ is a negative imaginary number [see Equations (13.8-3) and (13.8-4)] so that the two eigenvectors [of (13.9-13)] take the form

$$\underset{(\delta=0)}{\mathbf{E}_1(z)} = \begin{vmatrix} -1 \\ 1 \end{vmatrix} e^{-i(\beta-|\kappa|)z}$$

$$\underset{(\delta=0)}{\mathbf{E}_2(z)} = \begin{vmatrix} 1 \\ 1 \end{vmatrix} e^{-i(\beta+|\kappa|)z} \qquad (13.9\text{-}14)$$

$\mathbf{E}_1(z)$ is thus the odd symmetric mode while $\mathbf{E}_2(z)$ is even symmetric as depicted in Figure 13-25.

According to (13.9-11) the admixture, hence the profile of the supermode, depends on the phase velocity mismatch parameter δ. A situation may exist where the uncoupled dispersion curves of the individual guides may cross each other at some frequency ω_0, as shown in Figure 13-26. In the vicinity of ω_0 the supermode profile is thus a strong function of δ and, hence, of ω. If we approximate the mismatch parameter near ω_0 by $\delta = \text{const}\ (\omega - \omega_0)$, then the supermode's dispersion curves $\gamma_1(\omega)$ and $\gamma_2(\omega)$ are as shown in the figure. Also shown are the (super) mode profiles at ω_0 and at a frequency ω where $\delta(\omega) \gg \kappa$.

Since the supermode (i.e., eigenmode) description of the waveguide problem is formally equivalent to one that is based on individual waveguide coupled modes, it is instructive to consider how we might, for example, describe the phenomenon of directional coupling [see (13.8-7)] by means of our new point of view. To simplify matters, we assume $\delta = 0$ (phase-matching) and, referring to Figure 13-25, consider the case where at $z = 0$ power is fed into guide a (on the left) only. This boundary condition can be satisfied by expanding the total field at $z = 0$ as an equal admixture of the two

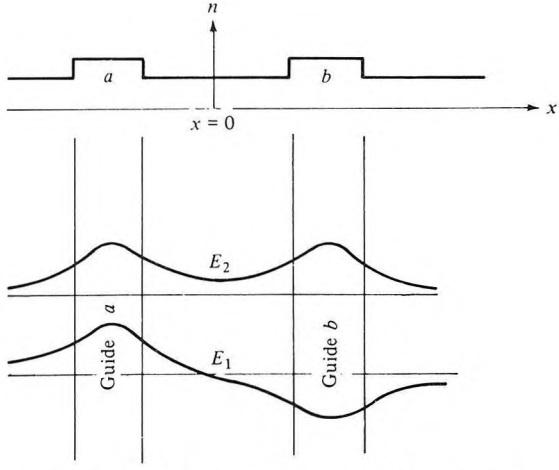

Figure 13-25 The transverse (x) field distribution of the two supermodes at the phase velocity matching ($\delta = 0$) condition of the parallel two-guide structure whose index of refraction profile is shown at the top.

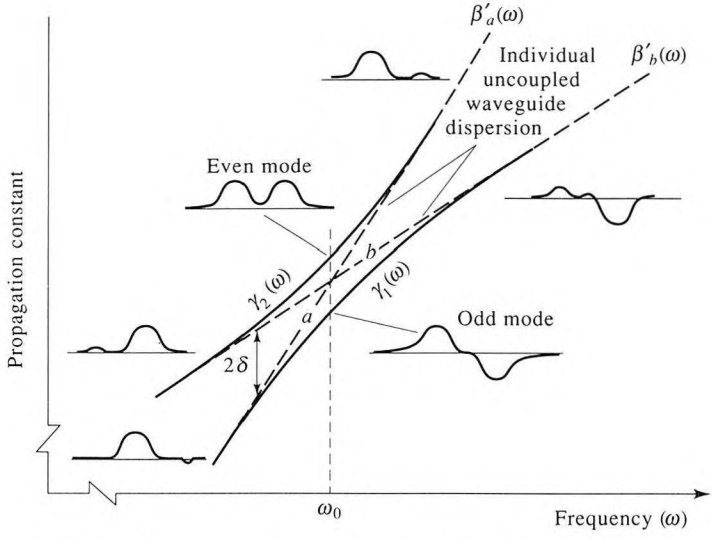

Figure 13-26 Some field distributions and the dispersion curves of the two lowest order "supermodes of a two-waveguide configuration near the phase-matching frequency (ω_0). The dashed curves correspond to the guide's dispersion at the absence of coupling.

supermodes (13.9-14) taken

$$\mathbf{E}_{\text{tot}}(0) = \mathbf{E}_1(0) + \mathbf{E}_2(0) = \begin{vmatrix} 0 \\ 2 \end{vmatrix} \tag{13.9-15}$$

It is also clear that if one were to add algebraically the fields of Figure 13-25, they would reinforce each other on the left and cancel each other on the right leading to the column vector in (13.9-15). Having established in (13.9-15) the proper admixture that satisfies the boundary condition at $z = 0$, we can determine the field at any z by simply inserting the z-dependence of each supermode.

$$\begin{aligned} \mathbf{E}_{\text{tot}}(z) &= \mathbf{E}_1(0)e^{-i(\beta-|\kappa|)z} + \mathbf{E}_2(0)e^{-i(\beta+|\kappa|)z} \\ &= \begin{vmatrix} \dfrac{i\kappa^*}{|\kappa|} \\ 1 \end{vmatrix} e^{-i(\beta-|\kappa|)z} + \begin{vmatrix} -\dfrac{i\kappa^*}{|\kappa|} \\ 1 \end{vmatrix} e^{-i(\beta+|\kappa|)z} \\ &= e^{-i(\beta-|\kappa|)z}[\mathbf{E}_1(0) + \mathbf{E}_2(0)e^{-i2|\kappa|z}] \end{aligned} \tag{13.9-16}$$

At a distance z where

$$|\kappa|z = \frac{\pi}{2}$$

the total field is

$$\mathbf{E}_{\text{tot}}\left(z = \frac{\pi}{2|\kappa|}\right) = e^{-i(\beta-|\kappa|)z}[\mathbf{E}_1(0) - \mathbf{E}_2(0)]$$

$$= e^{-i(\beta-|\kappa|)z}\begin{vmatrix} \dfrac{2i\kappa^*}{|\kappa|} \\ 0 \end{vmatrix} \tag{13.9-17}$$

so that the power is completely in the right waveguide. This exchange of power between the two guides takes place every $\Delta z = \pi/2|\kappa|$ just as predicted by the coupled-mode solution (13.8-7). Using the present point of view, however, we attribute the sloshing of power between guides to the difference of the phase constants $\gamma_2 - \gamma_1 = 2|\kappa|$ of the two supermodes leading to the factor $\exp(-i2|\kappa|z)$ in the last term of (13.9-16).

13.10 LASER ARRAYS [25, 26]

In Section 13.9 we showed that starting with the coupled-mode equations (13.8-6) for two adjacent and interacting waveguides we can obtain the supermode, i.e., the mode of the two-waveguide system. The same approach can be applied to the problem of finding the modes of an N-waveguide system. Semiconductor laser arrays [25, 26] are now widely used to increase the power output relative to that which is available from a single waveguide laser.

Consider a structure consisting of N adjacent waveguides as shown in Figure 13-27. For simplicity we assume that each waveguide can support

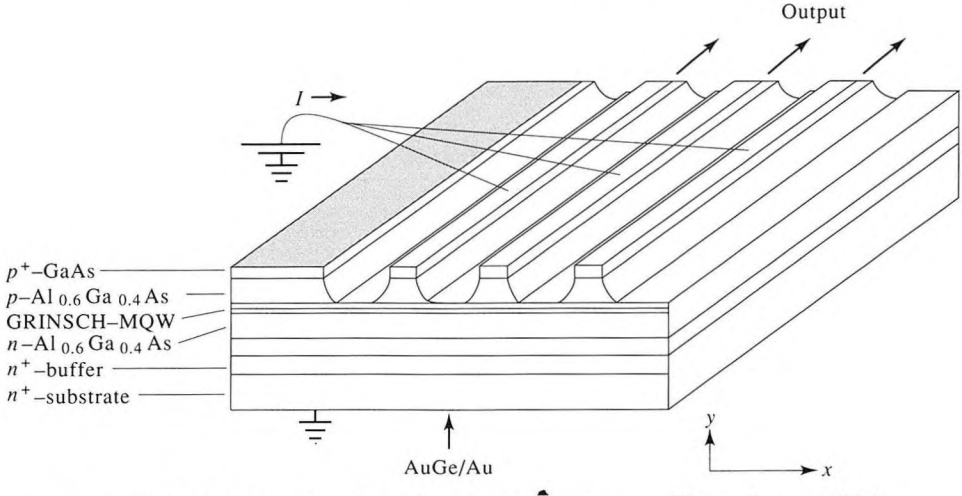

Figure 13-27 A three-channel semiconductor laser array. The active amplifying regions are GaAs quantum wells. The elliptical spots correspond to the near-field intensity pattern. (After Reference [27].)

one mode only. If we label the waveguides by 1, 2, . . . , N and take the normalized electric field mode solution of the isolated mth waveguide as $A_m\mathscr{E}_m(x, y)e^{-i\beta_m z}$, we can describe the total field at some arbitrary plane z as

$$\mathscr{E}(z) = \sum_m A_m(z)\mathscr{E}_m(x, y)e^{-i\beta_m z} \tag{13.10-1}$$

where the z dependence of A_m reflects the possible amplitude and phase coupling between the "individual" waveguide modes. If the waveguides were perfectly isolated from each other, the A_m's would be constant and *independent* of each other. The individual waveguide modes are subject to a normalization condition (13.2-6)

$$\frac{\beta_m}{2\omega\mu}\int_{-\infty}^{\infty} |\mathscr{E}_m(x, y)|^2 dxdy = 1 \tag{13.10-2}$$

so that the total power in the mth guide is $|A_m|^2$. The total field at z can be represented uniquely by the column vector

$$\mathbf{E}(z) \equiv \begin{vmatrix} A_1(z)e^{-i\beta_1 z} \\ A_2(z)e^{-i\beta_2 z} \\ \cdot \\ \cdot \\ \cdot \\ \cdot \\ \cdot \\ A_N(z)e^{-i\beta_N z} \end{vmatrix} \equiv \begin{vmatrix} E_1(z) \\ E_2(z) \\ \cdot \\ \cdot \\ \cdot \\ \cdot \\ \cdot \\ E_N(z) \end{vmatrix} \tag{13.10-3}$$

If we assume that each mode couples only to its immediate neighbors, then, in the manner of (13.9-1), the mode amplitudes $A_m(z)$ obey

$$\frac{dA_m}{dz} = \kappa_{m,m+1}A_{m+1}e^{i(\beta_m-\beta_{m+1})z} + \kappa_{m,m-1}A_{m-1}e^{i(\beta_m-\beta_{m-1})z} \tag{13.10-4}$$

From its definition in (13.10-3) and from (13.10-4), it follows that the component $E_m(z)$ of the vector $\mathbf{E}(z)$ obeys

$$\begin{aligned} \frac{dE_m}{dz} &= -i\beta_m A_m(z)e^{-i\beta_m z} + \frac{dA_m}{dz}e^{-i\beta_m z} \\ &= -i\beta_m A_m(z)e^{-i\beta_m z} + \kappa_{m,m+1}A_{m+1}e^{-i\beta_{m+1}z} \\ &\quad + \kappa_{m,m-1}A_{m-1}e^{-i\beta_{m-1}z} \end{aligned} \tag{13.10-5}$$

where, according to (13.9-1) and (13.8-3),

$$\kappa_{m,m+1} = -\kappa^*_{m+1,m} \tag{13.10-6}$$

The set of coupled equations (13.10-5) can be expressed, using the vector

definition of Equation (13.10-3), as

$$\frac{d\mathbf{E}}{dz} = \tilde{\mathbf{C}}E \tag{13.10-7}$$

$$\tilde{\mathbf{C}} = \begin{vmatrix} -i\beta_1 & \kappa_{1,2} & 0 & 0 & \cdots & 0 & 0 \\ \kappa_{2,1} & -i\beta_2 & \kappa_{2,3} & 0 & \cdots & 0 & 0 \\ 0 & \kappa_{3,2} & -i\beta_3 & \kappa_{3,4} & \cdots & 0 & 0 \\ \cdot & \cdot & \cdot & \cdot & & \cdot & \cdot \\ \cdot & \cdot & \cdot & \cdot & & \cdot & \cdot \\ \cdot & \cdot & \cdot & \cdot & & \cdot & \cdot \\ \cdot & \cdot & \cdot & \cdot & & \cdot & \cdot \\ 0 & 0 & 0 & 0 & \cdots & \kappa_{N,N-1} & -i\beta_N \end{vmatrix} \tag{13.10-8}$$

A propagating supermode, by definition, is a field solution that except for a phase factor $\exp(i\gamma z)$ to be determined, is independent of the propagation coordinate z. We can express it as

$$\mathbf{E}(z) = \mathbf{E}(0)e^{i\gamma z} \tag{13.10-9}$$

$$\frac{d\mathbf{E}}{dz} = i\gamma\mathbf{E}$$

which combined with (13.10-7) results in

$$(\tilde{\mathbf{C}} - i\gamma\tilde{\mathbf{I}})\mathbf{E} = 0 \tag{13.10-10}$$

where $\tilde{\mathbf{I}}$ is the identity $N \times N$ matrix. Equation (13.10-10) is a generalization of (13.9-7). If written out in detail, it becomes

$$\begin{aligned} &(C_{11} - i\gamma)E_1 + C_{12}E_2 + \cdots + C_{1N}E_N = 0 \\ &C_{21}E_1 + (C_{22} - i\gamma)E_2 + \cdots + C_{2N}E_N = 0 \\ &\quad\cdot \\ &\quad\cdot \\ &\quad\cdot \\ &\quad\cdot \\ &\quad\cdot \\ &\quad\cdot \\ &C_{N1}E_1 + C_{N2}E_2 + \cdots + (C_{NN} - i\gamma)E_N = 0 \end{aligned} \tag{13.10-11}$$

These are N homogeneous equations with N unknowns ($E_1, \ldots, E_N$) similar to Equation (13.9-8). The method of solution involves first finding the roots of the determinantal equation

$$\det|\tilde{\mathbf{C}} - i\gamma\tilde{\mathbf{I}}| = 0 \tag{13.10-12}$$

for the N eigenvalues $i\gamma_1, \ldots, i\gamma_N$. Each eigenvalue, say, $i\gamma_\nu$, is then used in (13.10-11) to obtain the corresponding eigenvector $\mathbf{E}^\nu$, which thus satisfies

$$(\tilde{\mathbf{C}} - i\gamma_\nu \tilde{\mathbf{I}})\mathbf{E}^\nu = 0 \tag{13.10-13}$$

The νth supermode (sometimes called the *array mode*) thus consists of a unique linear superposition of the individual waveguide modes $\mathscr{E}_m(x, y)$ with a fixed relative phase between any two of them. This combination propagates together with a *single* phase factor $\exp(i\gamma_\nu z)$. The total field of the νth array mode (supermode) can be written using (13.10-11), (13.10-3), and (13.10-9) as

$$\mathscr{E}^\nu(x,y,z) = \left[\sum_m E_m^\nu \mathscr{E}_m(x, y)\right] e^{i\gamma_\nu z} \tag{13.10-14}$$

The simple case of identical waveguides that are equally spaced deserves some special attention. In this case we have $\beta_1 = \beta_2 \cdots = \beta_N \equiv \beta$. We also have from (13.8-6)

$$\kappa_{m,m+1} = -\kappa_{m+1,m} = -i\kappa \tag{13.10-15}$$

Using the last relation we obtain directly from (13.10-12) and (13.10-11)

$$E_\ell^\nu = \sin\left(\ell \frac{\pi\nu}{N+1}\right) \qquad \begin{matrix} \ell = 1, 2, \ldots, N \\ \nu = 1, 2, \ldots, N \end{matrix} \tag{13.10-16}$$

$$\gamma_\nu = -\beta - 2\kappa \cos\left(\frac{\pi\nu}{N+1}\right) \tag{13.10-17}$$

where, we recall, E_ℓ^ν is the complex field amplitude in waveguide ℓ corresponding to supermode ν as in Equation (13.10-14). $-\gamma_\nu$ is, according to (13.10-9) the propagation constant of supermode ν.

Theoretical plots of a four-waveguide supermodes are shown in Figure 13-28. We note that only the fundamental $\nu = 0$ mode, in which all the channel fields possess the same phase, has a far-field consisting (mostly) of a single lobe centered on $\theta = 0^0$.

Semiconductor laser arrays of the type illustrated in Figure 13-27 have received a great deal of attention during the last few years due to their potential for combining coherently the power outputs of many lasers [25, 26]. Many different approaches to "encourage" the semiconductor laser array to oscillate only in its desirable (in-phase) fundamental mode have not been entirely successful [26].

To appreciate the connection between the near-field, say, at the output facet, and the far-field, we recall that according to (13.10-14) we can write the near field of the νth supermode measured at the output plane $z = L$ in the form of a phase-locked superposition of individual waveguide modes

$$\mathscr{E}^\nu(x, y, z) = \sum_{\ell=1}^{N} E_\ell^\nu \mathscr{E}_\ell(x, y) \exp(i\gamma_\nu z) \tag{13.10-18}$$

The amplitudes $E_\ell^\nu = E_\ell^\nu(0)$ are the solution of (13.10-11) for the νth mode. Let $E_\ell(\theta)$ be the far field of the ℓth channel by itself when $E_\ell^\nu = 1$ while $E_m^\nu = 0$ and $m \neq \ell$. With θ measured from the normal to the exit plane in the x-z plane, it follows from (13.10-18) by superposition that the far field of the νth supermode is

$$F^\nu(\theta) = \sum_{\ell=1}^{N} E_\ell^\nu E_\ell(\theta) \qquad (13.10\text{-}19)$$

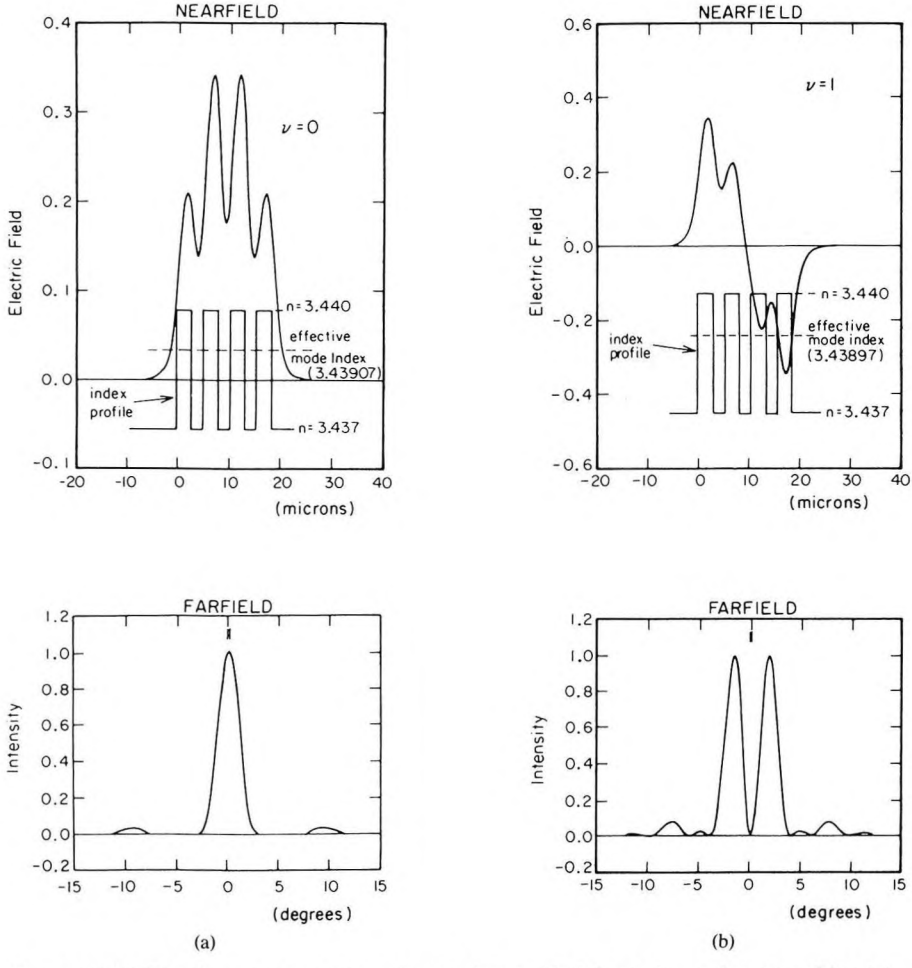

Figure 13-28 The four supermodes of an index-guided four-channel waveguide: (a) The lowest order (highest β) $\nu = 0$, mode. (b), (c), (d) The next three modes in decreasing order of β. The upper figure in each case shows the near field in relation to the channel array. The lower figure is that of the far-field intensity. The individual channel waveguides can support a single mode (each) only. (Courtesy of C. Lindsey)

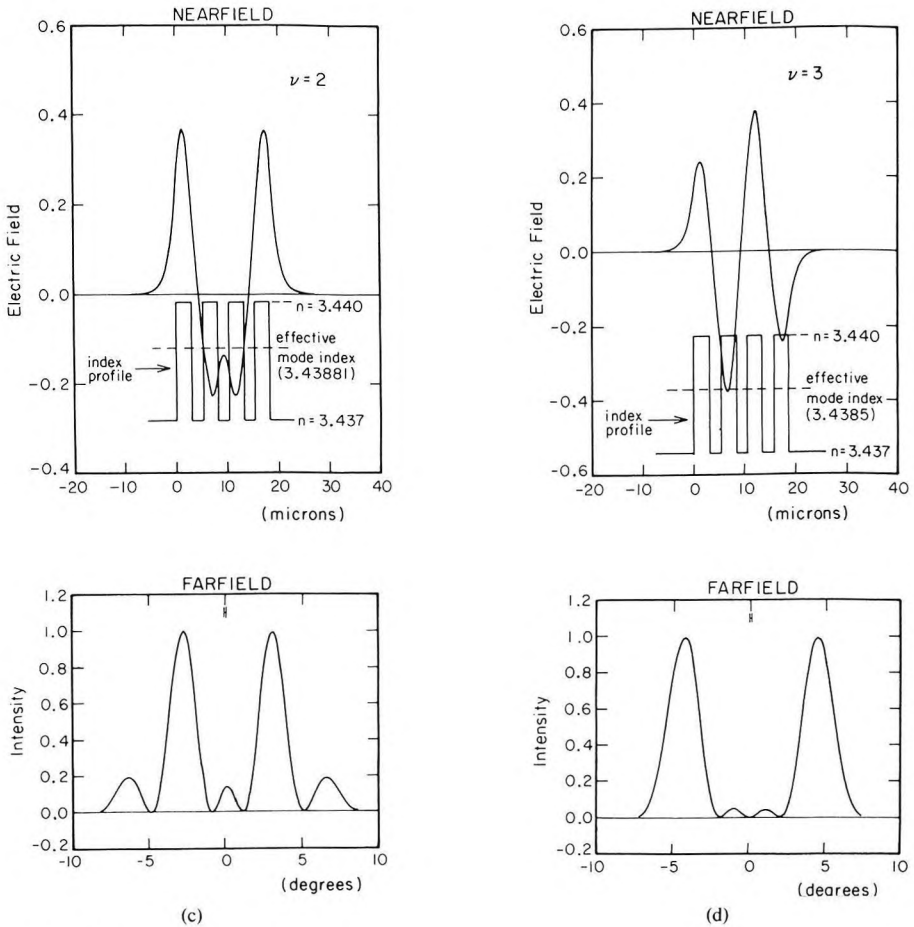

Figure 13-28 (*continued*)

In the, special but important, case of identical channels, we have

$$E_\ell(\theta) = E_{\ell+1}(\theta)e^{-ik_0 S\sin\theta} = E_0(\theta)e^{ik_0 \ell S\sin\theta}$$

where S is the separation between two channels so that $k_0 S\sin\theta$ is the extra phase delay in the far field between the fields arriving from two adjacent channels. From the last two equations

$$F^\nu(\theta) = E_0(\theta)\sum_{\ell=0}^{N-1} E_\ell^\nu e^{ik_0 \ell S\sin\theta} \qquad (13.10\text{-}20)$$

The far-field intensity pattern is

$$|F^\nu(\theta)|^2 = |E_0(\theta)|^2 G^\nu(\theta) \qquad (13.10.21)$$

with

$$G^{\nu}(\theta) \equiv \left| \sum_{\ell=0}^{N-1} E_{\ell}^{\nu} e^{ik_0 \ell S \sin\theta} \right|^2 \tag{13.10-22}$$

The "grating function" $G^{\nu}(\theta)$ is periodic in $\sin\theta$ (for $\theta \ll 1$ we can consider it to be periodic in θ) with a period $\Delta(\sin\theta) = 2\pi/(k_0 S)$. It corresponds physically to the radiation pattern in the far field of N point (i.e., "δ-function") sources spaced by S whose relative amplitudes are proportional to E_{ℓ}^{ν}. The grating function $G^0(\theta)$ of the fundamental ($\nu = 0$, i.e., $+++++$) mode of a five-element ($N = 5$) array is shown in Figure 13-29(a). The solid curve is based on amplitudes E_{ℓ}^0 obtained from a solution of (13.10-11). The dashed curve is a plot of $G^{\nu}(\theta)$ with $E_{\ell}^{\nu} = 1$, i.e., equal and in-phase amplitudes. The remaining curves show $G^{\nu}(\theta)$ of the high order supermodes. The limited

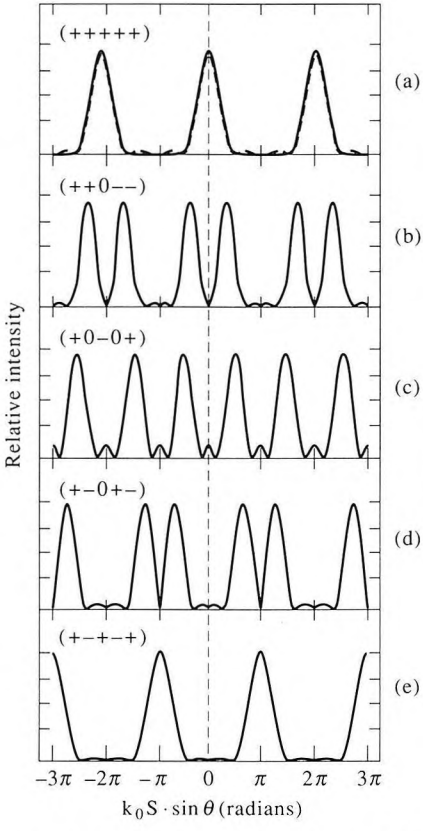

Figure 13-29 The grating functions G^{ν} of the five supermodes of a five-channel array. The dashed curve in (a) corresponds to an array of five equal amplitude ($E_i = 1$) radiators. (After Reference [25].)

angular spread of the optical beam as described by $F^{\nu}(\theta)$ is due to the finite angular extent of the single aperture radiation pattern $|E_0(\theta)|^2$ which is a factor in $F^{\nu}(\theta)$. In Problem 13.12 we show that to obtain a single-lobed, far-field pattern it is sufficient to have an aperture whose width satisfies $W \gtrsim S/2$.

Problems

13.1 Derive Equation (13.2-7).

13.2 Show that the form of Equation (13.7-10) is consistent with the conservation of the modes' power.

13.3 Derive the equations in (13.7-12).

13.4 Derive an expression for the modulation power of a transverse electrooptic waveguide modulator of length L and cross section $2\lambda \times 2\lambda$ (λ is the vacuum wavelength of the light). Compare to the bulk result ([9], p. 547). Estimate the power requirement for a $LiNbO_3$ modulator at $\lambda = 1$ μm, L = 5 mm.

13.5 Derive the condition for distributed feedback laser oscillation for the case of gain perturbation, that is, $\gamma_1 \neq 0$, $n_1 = 0$. Compare with the result of Reference [17].

13.6 Prove the orthogonality relation Equation (13.2-8). What happens to this relation if ε is complex?

13.7 Compare the ratio of the power propagating in the regions with an index n_1 to that of the total power for a TE_m and TM_m mode.

13.8 Show that in the case of electrooptic mode coupling in which $\beta_m^{TM} \neq \beta_m^{TE}$ [see Equation (13.7-10)], one can use a z periodic electrooptic constant or electric field to obtain phase matched operation. How would you accomplish this in practice? (Be bold and invent freely.)

13.9 Show that in the case of coupling between modes that carry power in opposite directions the conservation of total power condition becomes

$$\frac{d}{dz}(|A|^2 - |B|^2) = 0$$

which can be satisfied if instead of (13.7-10) we have

$$\frac{dA}{dz} = \kappa_{ab} B e^{-i(\beta_B - \beta_A)z}$$

$$\frac{dB}{dz} = \kappa_{ab}^* A e^{i(\beta_B - \beta_A)z}$$

Compare these equations with the contradirectional coupling case described by Equation (13.5-1).

13.10 Find the eigenmodes, as in (13.9-11), of a two-channel (waveguide) system with individual exponential gain constants γ_a and γ_b in each guide.

13.11 Referring to Figure 13-27 assume that the regions between the optical waveguides are highly absorbing. Explain qualitatively why the desirable $(++\cdots+)$ supermode has a smaller modal gain at a given injection current than the $(+-+-\cdots+)$ supermode.

13.12

a. Plot the array function $G^0(\theta)$ of a six-channel in-phase $(++++++)$ supermode taking $E_\ell^0 = 1$.
b. Using the diffraction result Equation (4.9-2), derive the far-field distribution $E_0(\theta)$ due to a single channel, say channel 0, whose near field is

$$\mathcal{E}_0(x, y) = \begin{cases} \cos\left(\dfrac{\pi x}{W}\right) & -W/2 \le x \le W/2 \\ 0 & \text{elsewhere} \end{cases}$$

c. Plot the far-field intensity distribution function $|F^0(\theta)|^2$ of the mode assuming $k_0 S = 6\pi$ and (1) $W = 0.05S$, (2) $W = 0.2S$, and (3) $W = 0.6S$. (S is the distance between the centers of two nearest-neighbor channels.) Obtain an approximate relation between the number of lobes in the far field and the ratio W/S.

13.13 Repeat Problem 13.12 for the $(+\ -\ +\ -\ +)$ mode, i.e., $E_0 = E_2 = E_{-2} = 1$, $E_1 = E_{-1} = -1$.

13.14 Estimate the coupling constant κ of the laser whose spontaneous emission spectrum is given in Figure 13-15(e).

13.15

a. Using a computer program ("Mathematica" will do nicely), plot the reflection coefficient [see Equation (13.6-16)] of a periodic amplifying waveguide as a function of $\Delta\beta L$, assuming $\kappa L = 0.4$. Let γL be the parameter and generate plots with $\gamma L = 2$, 2.9, 3.5, and 3.8.
b. Plot the equigain contours in the $\gamma L - \Delta\beta L$ plane as in Figure 13-12.

References

1. Yariv, A., and R. C. C. Leite, "Dielectric waveguide mode of light propagation in *p-n* junctions," *Appl. Phys. Lett.* 2:55, 1963.
2. Osterberg, H., and L. W. Smith, "Transmission of optical energy along surfaces," *J. Opt. Soc. Am.* 54:1073, 1964.

3. Hall, D., A. Yariv, and E. Garmire, "Optical guiding and electrooptic modulation in GaAs epitaxial layers," *Opt. Comm.* 1:403, 1970.
4. Shubert, R., and J. H. Harris, "Optical surface waves on thin films and their application to integrated data processors," *IEEE Trans. Microwave Theory Tech.* (1968 Symp. issue) MTT-16:1048–1054, Dec. 1968.
5. Miller, S. E., "Integrated optics, an introduction," *Bell Syst. Tech. J.* 48:2059, 1969.
6. Goell, J. E., "A circular harmonic computer analysis for rectangular dielectric waveguides," *Bell Syst. Tech. J.* 48:2133, 1968.
7. Marcatili, E. A. J., "Dielectric rectangular waveguide and directional couplers for integrated optics," *Bell Syst. Tech. J.* 48:2071, 1969.
8. Lotspeich, J. F., "Explicit general eigenvalue solutions for dielectric slab waveguides," *Appl. Opt.* 14:327, 1975.
9. Chapter 14, this book.
10. Hammer, J. M., D. J. Channin, and M. T. Duffy, "High speed electrooptic grating modulators," *RCA Technical Report,* unpublished.
11. Tien, P. K., R. Ulrich, and R. J. Martin, "Modes of propagating light in thin deposited semiconductor films," *Appl. Phys. Lett.* 144:291–293, 1969.
12. Yariv, A., "Coupled mode theory for guided wave optics," *IEEE J. Quant. Elec.* 9:919, 1973.
13. Kuhn, L., M. L. Dakss, P. F. Heidrich, and B. A. Scott, "Deflection of optical guided waves by a surface acoustic wave," *Appl. Phys. Lett.* 17:265, 1970.
14. Dixon, R. W., "The photoelastic properties of selected materials and their relevance to acoustic light modulators and scanners," *J. Appl. Phys.* 38:5149, 1967.
15. Stoll, H., and A. Yariv, "Coupled mode analysis of periodic dielectric waveguides," *Opt. Commun.* 8:5, 1973.
16. Flanders, D. C., H. Kogelnik, R. V. Schmidt, and C. V. Shank, "Grating filters for thin film optical waveguides," *Appl. Phys. Lett.* 24:194, 1974.
17. Kogelnik, H., and C. V. Shank, "Coupled wave theory of distributed feedback lasers," *J. Appl. Phys.* 43:2328, 1972.
18. Nakamura, M., A. Yariv, H. W. Yen, S. Somekh, and H. L. Garvin, "Optically pumped GaAs surface laser with corrugation feedback," *Appl. Phys. Lett.* 22:515, 1973.
19. K. Aiki, M. Nakamura, J. Umeda, A. Yariv, A. Katzir, and H. W. Yen, "GaAs-GaAlAs distributed feedback laser with separate optical and carrier confinement," *Appl. Phys. Lett.* 27:145, 1975.
20. Haus, H. A., and C. V. Shank, "Antisymmetric taper of distributed feedback lasers," *IEEE J. Quant. Elec.* QE-12:532, 1976.
21. Agrawal, G. P., and N. K. Dutta, *Long-Wavelength Semiconductor Lasers,* Van Nostrand and Reinhold Co., New York, 1986, Chapter 7.
22. Sasaki, S. M., M. Choy, and N. K. Cheung, "Effects of dynamic spectral behavior and mode partitioning of 1550 nm distributed feedback lasers on gigabit/sec transmission systems," *Electr. Lett.* 24:26, 1987.

23. Somekh, S., E. Garmire, A. Yariv, H. L. Garvin, and R. G. Hunsperger, "Channel optical waveguide directional couplers," *Appl. Phys. Lett.* 27:327–329, 1975.

24. Campbell, J. C., F. A. Blum, D. W. Shaw, and K. L. Lawley, "GaAs electro-optic directional-coupler switch," *Appl. Phys. Lett.* 27:202–205, 1975.

25. Kapon, E., J. Katz, and A. Yariv, "Supermode analysis of phase-locked arrays of semiconductor lasers," *Opt. Lett.* 9:125, 1984.

26. Scifres, D. R., R. D. Burnham, and W. Streifer, "Arrays of semiconductor lasers," *Appl. Phys. Lett.* 33:1015, 1978.

27. Kapon, E., C. Lindsey, J. Katz, S. Margalit, and A. Yariv, "Coupling mechanism of gain guided laser arrays," *Appl. Phys. Lett.* 44:389, 1984.